



# Translating phenotypic prediction models from big to small anatomical MRI data using meta-matching

Naren Wulan<sup>a,b,c</sup>, Lijun An<sup>a,b,c</sup>, Chen Zhang<sup>a,b,c</sup>, Ru Kong<sup>a,b,c</sup>, Pansheng Chen<sup>a,b,c</sup>, Danilo Bzdok<sup>d,e</sup>,  
Simon B. Eickhoff<sup>f,g</sup>, Avram J. Holmes<sup>h</sup>, B.T. Thomas Yeo<sup>a,b,c,i,j,k</sup>

<sup>a</sup>Centre for Sleep & Cognition & Centre for Translational Magnetic Resonance Research, Yong Loo Lin School of Medicine, National University of Singapore, Singapore, Singapore

<sup>b</sup>Department of Electrical and Computer Engineering, National University of Singapore, Singapore, Singapore

<sup>c</sup>N.1 Institute for Health, National University of Singapore, Singapore, Singapore

<sup>d</sup>Department of Biomedical Engineering, McConnell Brain Imaging Centre (BIC), Montreal Neurological Institute (MNI), Faculty of Medicine, School of Computer Science, McGill University, Montreal QC, Canada

<sup>e</sup>Mila – Quebec Artificial Intelligence Institute, Montreal, QC, Canada

<sup>f</sup>Institute for Systems Neuroscience, Medical Faculty, Heinrich-Heine University Düsseldorf, Düsseldorf, Germany

<sup>g</sup>Institute of Neuroscience and Medicine, Brain & Behavior (INM-7), Research Center Jülich, Jülich, Germany

<sup>h</sup>Department of Psychiatry, Brain Health Institute, Rutgers University, Piscataway, NJ, United States

<sup>i</sup>Integrative Sciences and Engineering Programme (ISEP), National University of Singapore, Singapore, Singapore

<sup>j</sup>Martinos Center for Biomedical Imaging, Massachusetts General Hospital, Charlestown, MA, United States

<sup>k</sup>Department of Medicine, Human Potential Translational Research Programme & Institute for Digital Medicine (WisDM), Yong Loo Lin School of Medicine, National University of Singapore, Singapore, Singapore

Corresponding Author: B.T. Thomas Yeo ([yeoyeo02@nus.edu.sg](mailto:yeoyeo02@nus.edu.sg))

## ABSTRACT

Individualized phenotypic prediction based on structural magnetic resonance imaging (MRI) is an important goal in neuroscience. Prediction performance increases with larger samples, but small-scale datasets with fewer than 200 participants are often unavoidable. We have previously proposed a “meta-matching” framework to translate models trained from large datasets to improve the prediction of new unseen phenotypes in small collection efforts. Meta-matching exploits correlations between phenotypes, yielding large improvement over classical machine learning when applied to prediction models using resting-state functional connectivity as input features. Here, we adapt the two best performing meta-matching variants (“meta-matching finetune” and “meta-matching stacking”) from our previous study to work with T1-weighted MRI data by changing the base neural network architecture to a 3D convolution neural network. We compare the two meta-matching variants with elastic net and classical transfer learning using the UK Biobank (N = 36,461), the Human Connectome Project Young Adults (HCP-YA) dataset (N = 1,017), and the HCP-Aging dataset (N = 656). We find that meta-matching outperforms elastic net and classical transfer learning by a large margin, both when translating models within the same dataset and when translating models across datasets with different MRI scanners, acquisition protocols, and demographics. For example, when translating a UK Biobank model to 100 HCP-YA participants, meta-matching finetune yielded a 136% improvement in variance explained over transfer learning, with an average absolute gain of 2.6% (minimum = −0.9%, maximum = 17.6%) across 35 phenotypes. Overall, our results highlight the versatility of the meta-matching framework.

**Keywords:** structural MRI, transfer learning, meta-matching, phenotypic prediction

Received: 12 December 2023 Revision: 28 May 2024 Accepted: 2 July 2024 Available Online: 17 July 2024



The MIT Press

© 2024 The Authors. Published under a Creative Commons  
Attribution 4.0 International (CC BY 4.0) license.

Imaging Neuroscience, Volume 2, 2024  
[https://doi.org/10.1162/imag\\_a\\_00251](https://doi.org/10.1162/imag_a_00251)

## 1. INTRODUCTION

An important goal in systems neuroscience is to understand how variation in brain structure relates to individual differences in behavior (Genon et al., 2022). Structural T1-weighted magnetic resonance imaging (MRI) is a noninvasive technique for examining the anatomy of the human brain, providing high contrast between gray and white matter (Gifford et al., 2020). Structural MRI is widely used to predict behavioral traits, clinical symptoms, and diagnostic categories in both healthy individuals and individuals with neuropsychiatric disorders (Arbabshirani et al., 2017; Bhagwat et al., 2019; Cohen et al., 2021; Ooi et al., 2022; Sabuncu et al., 2015). However, most prediction studies use datasets with fewer than a few hundred participants, leading to low reproducibility and inflated performance (Arbabshirani et al., 2017; Bzdok & Meyer-Lindenberg, 2018; Marek et al., 2022; Masouleh et al., 2019; Poldrack et al., 2020). Studies have shown that prediction performance increases with larger sample sizes (Chu et al., 2012; Cui & Gong, 2018; He et al., 2020; Schulz et al., 2020), but for investigations of certain clinical populations or focused neuroscience inquiries, small-scale datasets remain unavoidable. Here, to address this fundamental issue, we seek to establish a framework to translate prediction models from large-scale datasets to predict new nonbrain-imaging phenotypes in small-scale datasets based on anatomical T1-weighted images.

More specifically, given a large-scale anatomical MRI dataset ( $N > 10,000$ ) with multiple phenotypes, we seek to translate models trained from the large dataset to new unseen phenotypes in a small independent dataset ( $N \leq 200$ ). In machine learning, this problem is often referred to as meta-learning, lifelong learning, learning-to-learn, or few-shot learning (Andrychowicz et al., 2016; Fei-Fei et al., 2006; C. Finn et al., 2017; Ravi & Larochelle, 2016; Vanschoren, 2019), and is closely related to transfer learning (Hospedales et al., 2021; Weiss et al., 2016). Broadly speaking, meta-learning and transfer learning methods usually train a model on abundant data on a related problem, called the source dataset, and seek to translate knowledge learned from the large-scale dataset to the small dataset, called the target dataset. During the translation, a subset of the target dataset is typically used to adapt the pretrained model to the new sample. One distinction between meta-learning and transfer learning is that in transfer learning, the prediction problem in the target dataset can be same (Aderghal et al., 2018; Ghafoorian et al., 2017; Wee et al., 2019) or different (Dawud et al., 2019; Mehmood et al., 2021; Talo et al., 2019) from the source dataset. On the other hand, meta-learning always involves the translation of the prediction model to perform a *new* prediction problem in the target

dataset—providing the imaging neuroscience community with a versatile modeling framework that, once established, can be applied to a diversity of research goals.

In our previous study (He et al., 2022), we developed a simple “meta-matching” approach to translate prediction models from large datasets to improve the prediction of new phenotypes in small datasets. Meta-matching is grounded in the observation that many phenotypes are correlated, as demonstrated by previous studies identifying a small number of factors linking brain-imaging data to various nonbrain-imaging traits such as cognition, mental health, demographics, and other health attributes (Kebets et al., 2019; Miller et al., 2016; Smith et al., 2015; Xia et al., 2018). As a result, a phenotype X in a smaller-scale study is likely correlated, sharing a latent relationship, with a phenotype Y present in a larger population dataset. Therefore, a model trained to predict phenotype Y from the larger dataset might be predisposed to features useful for predicting phenotype X. Consequently, the predictive model of Y can be more effectively translated to predict phenotype X in the smaller study. As a demonstration of meta-matching (He et al., 2022), we trained a simple fully connected feedforward neural network to predict 67 nonbrain-imaging phenotypes from resting-state functional connectivity (RSFC) in the UK Biobank. The neural network was then translated using meta-matching to predict nonbrain-imaging phenotypes in the Human Connectome Project Young Adult (HCP-YA) dataset, yielding large improvements in prediction accuracies over classical kernel ridge regression (without meta-learning or transfer learning).

In the current study, we investigated whether the two best performing meta-matching variants (“meta-matching finetune” and “meta-matching stacking”) from our previous study (He et al., 2022) can be adapted to work with T1 MRI data. More specifically, given the different modalities (RSFC versus T1), the base neural network architecture was changed from a fully connected feedforward neural network to the simple fully convolutional network (SFCN; Peng et al., 2021). The SFCN was chosen because of its simplicity and top performance in the Predictive Analysis Challenge 2019 of brain age prediction (Peng et al., 2021). We compared the two meta-matching variants with classical elastic net and classical transfer learning using the UK Biobank (Miller et al., 2016; Sudlow et al., 2015), the Human Connectome Project Young Adults (HCP-YA) dataset (Van Essen et al., 2013), and the HCP-Aging dataset (Bookheimer et al., 2019; Harms et al., 2018).

It is worth mentioning that it is not obvious that meta-matching will confer great benefits in anatomical MRI, compared with RSFC (He et al., 2022). The reason is that RSFC-based prediction typically utilizes high-dimensional features derived from  $N \times N$  RSFC matrices, where  $N$  is the

number of brain parcels (or independent component analysis components). On the other hand, T1-based prediction can utilize low-dimensional  $N \times 1$  volumetric and/or thickness measures. Therefore, classical machine learning techniques (e.g., elastic net) might work really well in the small sample regime ( $\leq 200$  participants). Nevertheless, we found that meta-matching significantly outperformed classical elastic net and transfer learning, highlighting the versatility of the meta-matching framework.

## 2. METHODS

### 2.1. Datasets and preprocessing

In this section, we describe the datasets and preprocessing used in the current study. Table 1 summarizes the demographics and acquisition parameters of the three datasets we considered. We will evaluate meta-matching based on prediction accuracy when translating prediction models within the same dataset (UK Biobank), as well as across datasets, i.e., from the UK Biobank to the HCP-YA and HCP-Aging datasets. The very different age ranges between the HCP-YA and UK Biobank served as a strong test of the generalizability of meta-matching. All data collection and analysis procedures were approved by the respective institutional review boards (IRBs), including the National University of Singapore IRB for the analysis presented in this paper.

#### 2.1.1. UK Biobank

The UK Biobank (UKBB) dataset is a large-scale epidemiology study of over 500,000 adults from the United Kingdom (Alfaro-Almagro et al., 2018). The volunteers were recruited between 2006 and 2010 from 22 centers across the United Kingdom. Participants were asked to answer a variety of questionnaires about different aspects of health and lifestyle. In addition, a range of physiological measurements was also collected. We considered the same set of 36,848 participants and 67 nonbrain-imaging phenotypes (referred to as phenotypes henceforth; Table S1) from our previous study (He et al., 2022).

As part of the UK Biobank pipeline (Alfaro-Almagro et al., 2018), FreeSurfer recon-all was used to derive thickness and volume measures with the Desikan-

Killiany-Tourville (DKT40) cortical atlas (Klein & Tourville, 2012) and subcortical segmentation (Fischl et al., 2002). We considered the subset of regions present in most participants, yielding 164 morphometric measures, comprising intracranial volume (ICV) and thickness measures of 62 cortical regions, as well as volumes of 62 cortical regions and 39 subcortical gray-matter regions (Tables S4 and S5). After excluding participants who have dropped out from our previous study (He et al., 2022) and excluding participants without all 164 morphometric measures, we ended up with 36,461 participants. As a baseline, these 164 measures will be utilized by the elastic net algorithm for phenotypic prediction (see Section 2.3).

Furthermore, we used FMRIB's Linear Image Registration Tool (FLIRT) to transform the bias-field-corrected version of the brain-extracted T1 (from the UK Biobank provided preprocessing outputs) to the FSL MNI152 standard-space T1 template with 1 mm resolution (Jenkinson et al., 2002; Jenkinson & Smith, 2001). Each T1 image was cropped to dimensions 160 x 192 x 160, and then divided by the mean value within each image following Peng et al. (2021). The normalized T1 images will be used by a convolutional neural network for phenotypic prediction (Section 2.3). Table 2 summarizes the preprocessing steps for the 3D T1 images for the UK Biobank, HCP-YA, and HCP-Aging datasets.

#### 2.1.2. HCP young adult (HCP-YA) dataset

We utilized the Human Connectome Project Young Adult (HCP-YA) dataset (Van Essen et al., 2013), which included healthy young adults. We considered 1,019 participants and 35 nonbrain-imaging phenotypes, consistent with our previous study (He et al., 2022). The phenotypes are found in Table S2.

FreeSurfer recon-all from the HCP pipeline was used to derive thickness and volume measures with the DKT40 cortical atlas (Klein & Tourville, 2012) and ASEG subcortical segmentation (Fischl et al., 2002). We considered the subset of regions present in most participants, yielding 166 morphometric measures, comprising intracranial volume (ICV) and thickness measures of 62 cortical regions, as well as volumes of 62 cortical regions and 41 subcortical gray-matter regions (Tables S4 and S5). We note that the difference in the number of morphometric measures

**Table 1.** Summary of demographics and acquisition parameters of the three datasets used in the current study.

	Age	Sex (M/F)	Scanner(s)	Resolution
UK Biobank	45-82	53%/47%	Siemens Skyra 3T scanner	1 mm
HCP-YA	22-35	47%/53%	Customized Skyra 3T scanner	0.7 mm
HCP-aging	36-100	44%/56%	Siemens Prisma 3T scanner	0.8 mm

**Table 2.** Summary of preprocessing steps for the 3D T1 images for the UK Biobank, HCP-YA, and HCP-Aging datasets.

Step #	UK Biobank	HCP pipeline
1	Gradient distortion correction	Gradient distortion correction
2	Brain extraction (BET) and cut down FOV.	Averaging of the same files (if multiple scans of the same modality exist)
3	Registration to standard space (linear) (FLIRT)	AC-PC alignment
4	Registration to standard space (nonlinear) (FNIRT)	Image FNIRT-based brain extraction
5	Create brain mask from MNI152_T1_1 mm, then do brain extraction	T2w to T1w image registration
6	Defacing	Readout distortion correction
7	Bias correction (the bias field is estimated using FAST)	Bias field correction
8	Tissue and subcortical structure segmentation	Linear and nonlinear atlas registration to MNI152

between the UK Biobank and HCP-YA datasets (164 vs. 166) arose because the 5th-Ventricle and non-WM-hypointensities were missing in most participants from the UK Biobank dataset. As a baseline, these 166 measures will be utilized by the elastic net algorithm for phenotypic prediction (see [Section 2.3](#)).

Moreover, we considered T1 images of 0.7 mm resolution which had been transformed to FSL MNI152 space by FLIRT from the HCP PreFreesurfer pipeline ([Glasser et al., 2013](#)), which included gradient distortion correction, brain extraction, and readout distortion correction. We noted the files of two participants were missing in the HCP filesystem, so we ended up with 1,017 participants. Each T1 image was downsampled to 1 mm, cropped to dimensions 160 x 192 x 160, and then divided by the mean value within each image following [Peng et al. \(2021\)](#). The processed T1 images will be used by a convolutional neural network for phenotypic prediction ([Section 2.3](#)).

### 2.1.3. HCP-aging dataset

Besides the HCP-YA dataset, we also used the Human Connectome Project Aging (HCP-Aging) dataset ([Bookheimer et al., 2019](#); [Harms et al., 2018](#)) consisting of healthy participants. We manually selected commonly used nonbrain-imaging phenotypic measures across cognition, emotion, motor, sensor, and life experience, resulting in 45 phenotypes (Table S3). By only considering participants with at least 90% of the phenotypes, we ended up with 656 participants (out of 725 participants). Similar to the HCP-YA dataset, we used the same 166 morphometric measures generated by the FreeSurfer recon-all procedure from the HCP pipeline. Moreover, we considered T1 images of 0.8 mm resolution, which had been transformed to FSL MNI152 space by FLIRT from the HCP PreFreesurfer pipeline ([Glasser et al., 2013](#)), which included gradient distortion correction, brain extraction, and readout distortion correction. Each T1 image was downsampled to 1 mm, cropped to dimensions 160 x 192 x 160, and then divided by the mean

value within each image following [Peng et al. \(2021\)](#). The processed T1 images will be used by a convolutional neural network for phenotypic prediction ([Section 2.3](#)).

## 2.2. Data split for different analyses

We performed two sets of analyses. First, we benchmarked meta-matching within the UK Biobank. Second, we translated predictive models from the UK Biobank to the HCP-YA and HCP-Aging datasets.

### 2.2.1. Data split within the UK Biobank

For the UK Biobank analysis, we considered 36,461 participants with T1 structural MRI and 67 phenotypes. As illustrated in [Figure 1](#), we randomly split the data into a meta-training set comprising 26,573 participants with 33 phenotypes, as well as a meta-test set comprising 9,888 participants with 34 phenotypes. There was no overlap between the participants and phenotypes across the meta-training set and meta-test set.

We further randomly split the meta-training set into a training set with 21,258 participants (80% of 26,573 participants) and a validation set with 5,315 participants (20% of 26,573 participants). The validation set was used for tuning hyperparameters of the predictive models.

For the meta-test set, we randomly split 9,888 participants into K participants (K-shot) and 9,888-K participants, where K had a value of 10, 20, 50, 100, and 200. The group of K participants mimicked traditional small-N studies. Various trained models from the meta-training set were translated to the meta-test set using the K participants. The models were then evaluated using the remaining N - K participants. Each random K-shot split was repeated 100 times to ensure stability.

### 2.2.2. Data split scheme for cross-dataset analyses

To translate predictive models from the UK Biobank to other datasets, we considered the HCP-YA and



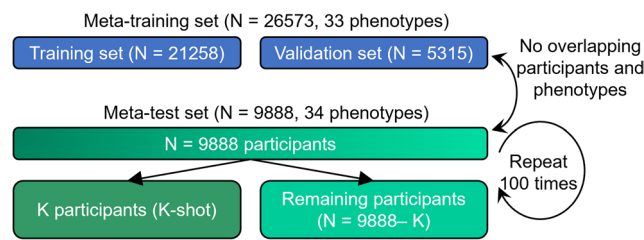


**Fig. 1.** Data split scheme for within-UK Biobank analysis. The UK Biobank dataset was divided into a meta-training set comprising 26,573 participants and 33 phenotypes, as well as a meta-test set comprising 9,888 participants and 34 other phenotypes. There was no participant or phenotype overlap between the meta-training and meta-test sets. The meta-test set was, in turn, split into K participants ( $K = 10, 20, 50, 100$ , and  $200$ ) and remaining  $9,888 - K$  participants. The group of K participants mimicked studies with traditionally common sample sizes. Various trained models from the meta-training set were translated to the meta-test set using the K participants. The models were then evaluated using the remaining  $N - K$  participants. This random split was repeated 100 times for robustness.

HCP-Aging datasets. As illustrated in [Figure 2](#), the meta-training set comprised all 36,461 participants with all 67 phenotypes from the UK Biobank dataset. The first meta-test set consisted of 1,017 participants with 35 phenotypes from the HCP-YA dataset. The second meta-test set consisted of 656 participants with 45 phenotypes from the HCP-Aging dataset. There was no overlap between the participants and phenotypes across the meta-training and meta-test sets because they were from totally different datasets. For the meta-training set, we further randomly split it into a training set with 29,169 participants (80% of 36,461 participants) and a validation set with 7,292 participants (20% of 36,461 participants). The validation set was used for tuning hyperparameters of the predictive models.

For the HCP-YA dataset, we randomly split 1,017 participants into K participants (K-shot) and  $1,017 - K$  participants, where K had a value of 10, 20, 50, 100, and 200. Various trained models from the meta-training set were translated to the meta-test set using the K participants. The models were then evaluated using the remaining  $N - K$  participants. Each random K-shot split was repeated 100 times to ensure stability. The same procedure was applied to the HCP-Aging dataset.

### 2.3. Predictive models

[Figure 3](#) provides an overview of the different approaches we will compare. Across all approaches, we z-normalize each nonimaging phenotype to have zero mean and unit variance across participants. More specifically, in the

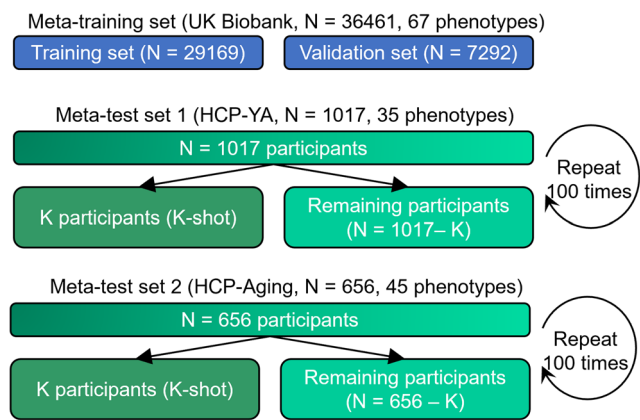


**Fig. 2.** Data split scheme for cross-dataset analysis. The meta-training set comprised 36,461 UK Biobank participants and 67 phenotypes. The first meta-test set comprised 1,017 HCP-YA participants and 35 phenotypes. The second meta-test set comprised 656 HCP-Aging participants and 45 phenotypes. Each meta-test was, in turn, split into K participants ( $K = 10, 20, 50, 100$ , and  $200$ ) and the remaining participants. The group of K participants mimicked studies with traditionally common sample sizes. Various trained models from the meta-training set were translated to the meta-test set using the K participants. The models were then evaluated using the remaining  $N - K$  participants. This random split was repeated 100 times for robustness.

case of the meta-training set, the mean and standard deviation were computed using all the participants to apply the z-normalization. In the case of the meta-test set, for each phenotype, the mean and standard deviation were computed from the K participants and subsequently carried over to the full meta-test set comprising the K participants and the remaining  $N - K$  test participants.

Following our previous study ([He et al., 2022](#)), statistical difference between algorithms was evaluated using a bootstrapping approach (more details in Supplementary Methods S2). More specifically, we will compare both meta-matching variants ([Sections 2.3.3](#) and [2.3.4](#)) with the two baselines ([Sections 2.3.1](#) and [2.3.2](#)). Multiple comparisons were corrected using a false discovery rate (FDR) of  $q < 0.05$ . FDR was applied to all K-shots, across all comparisons and both evaluation metrics: Pearson's correlation and coefficient of determination (COD). Formula for COD ([Feilong et al., 2021](#)) is found in Supplementary Methods S3.

#### 2.3.1. Baseline 1: elastic net

As a baseline, we used thickness and volumetric measures as input features to predict individuals' phenotypes using elastic net ([Fig. 3](#)). Elastic net is a linear regression model with an L1 lasso and L2 ridge regularization terms

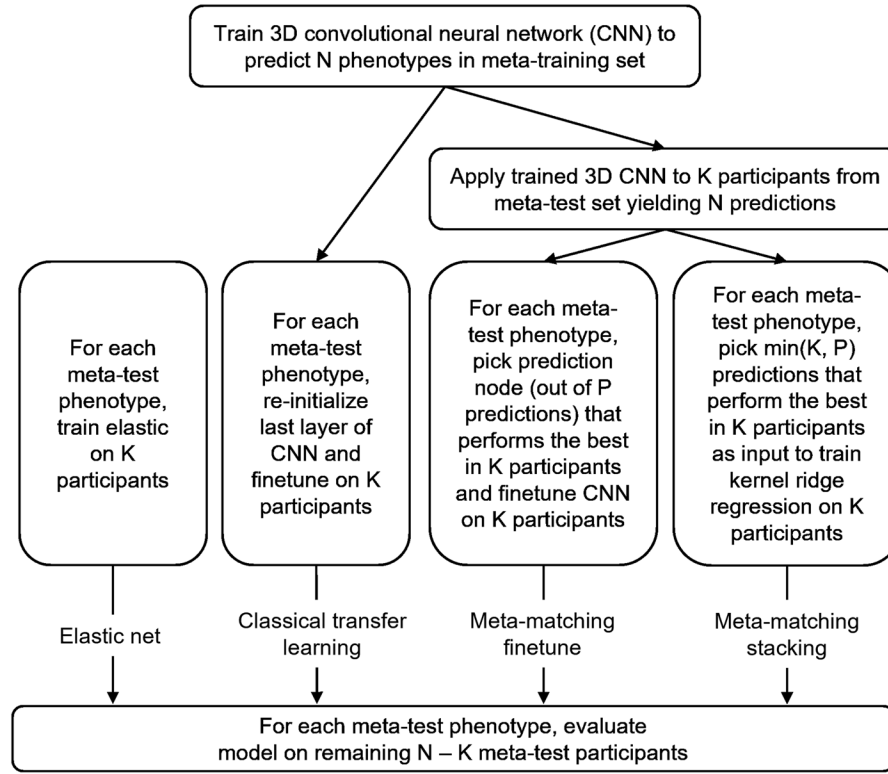


**Fig. 3.** Overview of different approaches. We considered two baselines: elastic net and classical transfer learning. We proposed two meta-matching variants: meta-matching finetune and meta-matching stacking.

(Zou & Hastie, 2005). Here, we chose elastic net as a baseline because previous studies have suggested that the elastic net yielded strong prediction performance in phenotypic prediction for brain MRI data (Ooi et al., 2022; Peng et al., 2021; Pervaiz et al., 2020).

As a reminder, we had 62 cortical regions and 39 subcortical gray-matter regions in the UK Biobank (Section 2.1.1). The cortical regions yielded cortical thickness and volumetric measures, while the subcortical regions yielded volumetric measures. Together with the intracranial volume, this results in  $1 + 62 \times 2 + 39 = 164$  morphometric features that were fed into the elastic net. In the case of the HCP-YA and HCP-Aging datasets, we had 62 cortical regions and 41 subcortical gray-matter regions (Sections 2.1.2 and 2.1.3), yielding  $1 + 62 \times 2 + 41 = 166$  morphometric features.

We note that the range of values is very different for volumetric and thickness measures. Therefore, given  $K$  participants from the meta-test set, the morphometric (volumetric and thickness) measures were z-normalized based on the mean and standard deviation computed from the  $K$  participants. We note that the morphometric measures of the  $N - K$  participants were also z-normalized using the mean and standard deviation computed from the  $K$  participants. The z-normalized morphometric measures were used as input to train the elastic net model on the  $K$  participants.

More specifically, we performed fivefold cross-validation on the  $K$  participants with different combinations of the hyperparameters  $\lambda_1$  and  $\lambda_2$  (which controlled the strength of the L1 and L2 regularizations). We used COD to evaluate prediction performance to choose the best hyperparameters for  $\lambda_1$  and  $\lambda_2$  across the fivefold cross-validation.

The best hyperparameters  $\lambda_1$  and  $\lambda_2$  were then used to train the elastic net model using all  $K$  participants. The trained elastic net model was then applied to the remaining  $N - K$  test participants in the meta-test set. Pearson's correlation and the COD were used to evaluate prediction performance. This procedure was repeated for each of the 100 random splits.

### 2.3.2. Baseline 2: classical transfer learning

To perform classical transfer learning, we first trained a simple fully convolutional network (SFCN) introduced by Peng et al. (2021) in the meta-training set to jointly predict all the available meta-training phenotypes.

The input to the SFCN is the mean-normalized T1 image affine transformed to MNI152 standard space (Section 2.1). The SFCN's convolutional neural network (CNN) architecture was based on VGG (Simonyan & Zisserman, 2014) and used a fully convolutional structure (Long et al., 2015). We chose the SFCN given its

simplicity and top performance in the Predictive Analysis Challenge 2019 of brain age prediction (Peng et al., 2021). In the original study (Peng et al., 2021), the last layer comprised 40 nodes that represented the predicted probability of the age interval that a participant's age falls into. Here, we modified the last layer to predict P phenotypes simultaneously. P is equal to 33 in the within-UK Biobank analysis (Fig. 1) and P is equal to 67 in the cross-dataset analysis (Fig. 2).

Figure 4 shows the overall network architecture. The 3D CNN consisted of several convolutional blocks for feature extraction. Each feature extraction block (except the last block) consisted of a 3D convolutional layer, a batch normalization layer, a max pooling layer, and a ReLU activation layer. The last block was similar to the previous blocks but without the max pooling layer. The feature maps from the last block were fed into an average pooling layer (green in Fig. 4).

Since the elastic net utilized ICV as one of the features, while affine registration of T1 to MNI152 space removed this information, for the comparison to be comparable, we concatenated z-normalized ICV with the outputs of the average pooling layer. More specifically, for both meta-training and meta-test sets, ICV of each participant was z-normalized using the mean and standard deviation computed from the participants of the training set within the meta-training set. The concatenated features were then fed into a dropout layer and then went through a 3D convolution layer with  $1 \times 1 \times 1$  kernel size to produce the final outputs.

The hyperparameters of the CNN were empirically determined based on the meta-training set from the within-UK Biobank analysis (Fig. 1A). Both within-UK Biobank and cross-dataset analyses used the same set of hyperparameters. More details about model architecture and hyperparameters (e.g., the number of blocks, number of

channels per block, and kernel size per block) can be found in Supplementary Methods S1.

The same transfer learning procedure was used for both within-UK Biobank analysis and cross-dataset analysis (Fig. 3). The only difference is that the within-UK Biobank analysis used a CNN model trained on 26,573 participants and 33 phenotypes, while the cross-dataset analysis used a CNN model trained on 36,461 participants and 67 phenotypes.

To perform transfer learning, we first replaced the last layer of the 3D CNN model (trained on the meta-training set) with a new convolutional layer with  $1 \times 1 \times 1$  kernel size and one output node. The new convolutional layer was initialized with random weights. For each meta-test phenotype, the last two layers of the CNN model were then finetuned on K participants in the meta-test set, while the weights of the remaining layers were frozen.

The optimal learning rate was determined using grid search and fivefold cross-validation on the K participants. After choosing the optimal learning rate, it was then used to train a final model using all K participants. For both the fivefold cross-validation and the final round of finetuning, the maximum finetuning epochs were set to be 50 with 80% of K participants used for training and 20% used to evaluate validation loss for early stopping, to reduce the possibility of overfitting. This final trained model was evaluated in the remaining  $N - K$  participants in the meta-test set. Pearson's correlation and COD were used to evaluate the prediction performance. This procedure was repeated for each of the 100 random splits.

### 2.3.3. Meta-matching finetune

As an alternative to transfer learning, we considered the "meta-matching finetune" approach (Fig. 3) introduced in our previous study (He et al., 2022). To explain the meta-matching finetune procedure in the current study, we will focus on the experimental setup for the within-UK Biobank analysis.

Recall from Section 2.3.2 that we have trained a 3D CNN model to predict 33 phenotypes in the meta-training set from the UK Biobank. Given K participants from the meta-test set, we applied the CNN yielding 33 predictions. For each meta-test phenotype (out of 34 phenotypes), we calculated the accuracy (COD) with each of the 33 predictions for the K participants. The output node of the CNN model with the best COD was chosen, while the remaining 32 nodes were removed. The last two layers of the CNN model were finetuned using the K participants, while the weights of the remaining layers were frozen.

Therefore, the difference between meta-matching finetune and classical transfer learning (Section 2.3.2) is the initialization of the last layer. Classical transfer learning

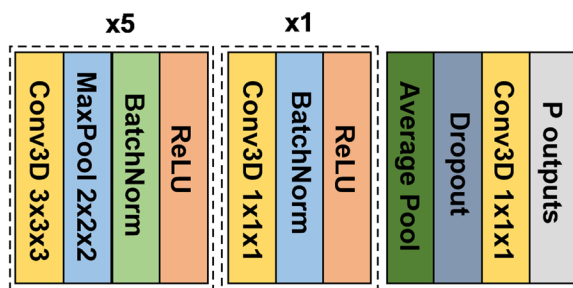


**Fig. 4.** Network architecture of the Simple Fully Convolutional Neural Network (SFCN) model (Peng et al., 2021) adapted to the current study. In the original study (Peng et al., 2021), the last layer comprised 40 nodes that represented the predicted probability of the age interval that a participant's age falls into. Here, we modified the last layer to predict P phenotypes simultaneously.

randomly initialized the last layer, while meta-matching finetune initialized the last layer by choosing the “closest” phenotypic prediction model from the meta-training set.

The optimal learning rate for finetuning was determined using grid search and fivefold cross-validation on the K participants. After choosing the optimal learning rate, it was then used to train a final model using all K participants. For both the fivefold cross-validation and the final round of finetuning, the maximum finetuning epochs were set to be 50 with 80% of K participants used for training and 20% used to evaluate validation loss for early stopping, to reduce the possibility of overfitting.

This final trained model was evaluated in the remaining  $N - K$  participants in the meta-test set. Pearson’s correlation and COD were used to evaluate the prediction performance. This procedure was repeated for each of the 100 random splits. The same procedure was used for both the within-UK Biobank analysis and cross-dataset analysis (Fig. 3). The only difference was that the within-UK Biobank analysis used a CNN model trained on 26,573 participants and 33 phenotypes, while the cross-dataset analysis used a CNN model trained on 36,461 participants and 67 phenotypes.

### 2.3.4. Meta-matching stacking

We also considered the meta-matching stacking approach (Fig. 3) introduced in our previous study (He et al., 2022). To explain the meta-matching stacking procedure in the current study, we will again focus on the experimental setup for the within-UK Biobank analysis.

Recall from Section 2.3.2 that we have trained a 3D CNN model to predict 33 phenotypes in the meta-training set from the UK Biobank. Given K participants from the meta-test set, we applied the CNN yielding 33 predictions. For each meta-test phenotype (out of 34 phenotypes), we calculated the accuracy (COD) with each of the 33 predictions for the K participants, and selected the top M predictions. The value of M was set to be the minimum of K and 33 to reduce overfitting. For example, when  $K = 20$ , then M was set to be 20. When  $K = 50$ , then M was set to be 33.

A stacking procedure was then performed (Breiman, 1996; Wolpert, 1992), in which a kernel ridge regression (KRR) model was trained on K participants using the M predictions as input to predict the meta-test phenotype. Similar to our previous study (He et al., 2022), we used the correlation kernel. The hyperparameter  $\lambda$  was tuned using grid search and fivefold cross-validation on the K participants. The optimal  $\lambda$  was then used to train a final KRR model using all K participants.

The trained KRR model was then applied to the remaining  $N - K$  participants in the meta-test set. Pearson’s

correlation and the COD were used to evaluate the prediction performance. This procedure was repeated for each of the 100 random splits.

## 2.4. Deep neural network implementation

The deep neural network was implemented using PyTorch (Paszke et al., 2017) and computed on NVIDIA RTX 3090 GPUs with CUDA 11.0. More details are found in Supplementary Methods S1.

## 2.5. Model interpretation

Future studies using our pretrained models would have to interpret the resulting meta-matching models. Therefore, to illustrate how meta-matching models can be interpreted, similar to our previous study (He et al., 2022), we utilized the Haufe transform (Haufe et al., 2014) to interpret the meta-matching stacking prediction of the Rey Auditory Verbal Learning Test (RAVLT) score and Montreal Cognitive Assessment (MOCA) in the HCP-Aging dataset for  $K = 100$  participants.

For a predictive model with T1 structural MRI as input and phenotype as output, Haufe transform produces a feature importance value for each voxel. A positive (or negative) predictive feature value implied that higher T1 intensity was related to predicting greater (or lower) phenotypic score.

More specifically, for each phenotype, Haufe transform was calculated as the covariance between the phenotype’s prediction based on the meta-matching stacking model and the intensity value of each T1 voxel (across the 100 participants), yielding a 3D volume. The 3D volumes were averaged across the 100 random sampling of 100 participants, and were then visualized in MNI152 space.

We chose cognitive measures from the HCP-Aging dataset because there is a vast literature studying the relationships between aging and brain structures. As such, we expected that smaller hippocampal volume and larger ventricular size were predictive of worse cognition. However, because the model was trained on T1 intensities, careful inference is necessary to link the feature importance values of T1 intensities with more neuroanatomically grounded interpretations, e.g., how interindividual variation in hippocampal volume predicts cognition.

## 2.6. Computational costs

Meta-matching training comprised two stages. The first stage was to train the 3D CNN model on the meta-training set. The second stage adapted the model to K participants from a new target dataset. Finally, the adapted model was tested on the remaining  $N - K$  participants in



the meta-test set, where  $N$  was the total number of participants in the meta-test set.

In our study, the 3D CNN model was trained on the meta-training set, using a single GPU (RTX3090 with 24 GB GPU memory). The whole training procedure took around 5 days. For the second stage involving  $K$  meta-test participants, meta-matching stacking required a single forward pass through the 3D CNN model, followed by training a KRR model on the  $K$  participants for each target phenotype. For each random sampling of  $K$  participants, for each value of  $K$  and for each phenotype, the training time was around 0.2 seconds (inclusive of the fivefold cross-validation to select the best hyperparameter). Evaluating the trained meta-matching stacking model on the  $N - K$  participants was a lot faster. For each value of  $K$  and each phenotype, evaluation for each random sampling of  $K$  participants required around 0.0007 seconds per 100 test participants.

On the other hand, the computational costs for meta-matching finetune and classical transfer learning were about the same, but a lot more than meta-matching stacking. For each random sampling of  $K$  participants and for each phenotype, the training time for meta-matching finetune (or transfer learning) was about 5 seconds for  $K = 10$  or 20, and about 30 seconds for  $K = 50$ , 100, or 200 (inclusive of the fivefold cross-validation to select the best hyperparameter). Evaluation in the  $N - K$  participants was a lot faster. For each value of  $K$  and each phenotype, evaluation for each random sampling of  $K$  participants required around 0.0193 seconds per 100 test participants.

Because of the expensive training costs for meta-matching finetune and classical transfer learning, the bootstrapping procedure to obtain  $p$  values could not be applied to meta-matching finetune and classical transfer learning. With one GPU, the entire training procedure of the within-UK Biobank, HCP-YA, and HCP-Aging analyses with 1000 bootstraps would require around  $(5 \text{ seconds} \times 2 + 30 \text{ seconds} \times 3) \times 1000 \text{ bootstraps} \times 114 \text{ phenotypes} = 11,400,000 \text{ seconds}$  or 132 days. Doing this for both meta-matching finetune and classical transfer learning would then require 264 days. On our computing facility, we might on average be able to utilize four GPUs (depending on load), so the total run time would be  $264 / 4 = 66 \text{ days}$ .

In the case of elastic net, with 164 (or 166) morphometric features, for each random sampling of  $K$  participants and for each phenotype, the training time was about 3 seconds for  $K = 10$  or 20, and was about 6 seconds for  $K = 50$ , 100, or 200. For each value of  $K$  and each phenotype, evaluation for each random sampling of  $K$  participants required around 0.0028 seconds per 100 test participants.

### 3. RESULTS

#### 3.1. Meta-matching outperforms elastic net and transfer learning within the UK Biobank

Four approaches (elastic net, classical transfer learning, meta-matching finetune, and meta-matching stacking) were applied to the UK Biobank to predict 34 meta-test phenotypes. The models were trained or adapted based on  $K$  participants and then evaluated on the remaining  $9,888 - K$  participants (Fig. 1).

Figures 5A and 6A show the Pearson's correlation and COD, respectively, averaged across all 34 meta-test phenotypes. Each boxplot represents 100 random samplings of  $K$  participants. Figures 5B and 6B show the outcomes of the statistical tests obtained by a bootstrapping procedure (Supplementary Methods S2 and Figure S1). The actual  $p$  values are reported in Table S6. Colors indicate effect sizes of differences (Cohen's  $D$ ) between approaches.

In the case of Pearson's correlation (Fig. 5), both meta-matching finetune and meta-matching stacking greatly outperformed elastic net and classical transfer learning for all values of  $K$ . Meta-matching stacking was statistically better than meta-matching finetune for  $K \geq 100$ .

In the case of COD (Fig. 6), both meta-matching finetune and meta-matching stacking greatly outperformed elastic net for all values of  $K$ . For  $K \leq 20$ , classical transfer learning was numerically better but not statistically better than meta-matching stacking. From  $K \geq 50$ , meta-matching stacking was numerically better than transfer learning with statistical significance from  $K = 100$  onward.

On the other hand, for  $K = 10$ , classical transfer learning was numerically better than meta-matching finetune, while meta-matching finetune was better than classical transfer learning for the remaining other values of  $K$  with large effect sizes (light green in Fig. 6B). We note that there was no statistical test between meta-matching finetune and classical transfer learning because of the huge computational cost of the two approaches, so no bootstrapping was performed for either approach.

Another relevant point is that COD for all approaches was negative for  $K = 10$ . COD was positive for meta-matching finetune for  $K = 20$  onward, and positive for meta-matching stacking for  $K = 50$  onward. This suggests that absolute prediction accuracy (i.e., COD) is difficult even with meta-learning or transfer learning, when the sample size is very small.

Overall, meta-matching was better than elastic net for all values of  $K$  for both evaluation metrics (Pearson's correlation and COD). On the other hand, meta-matching compared favorably with respect to transfer learning for all values of  $K$  for Pearson's correlation and for larger values of  $K$  for COD.

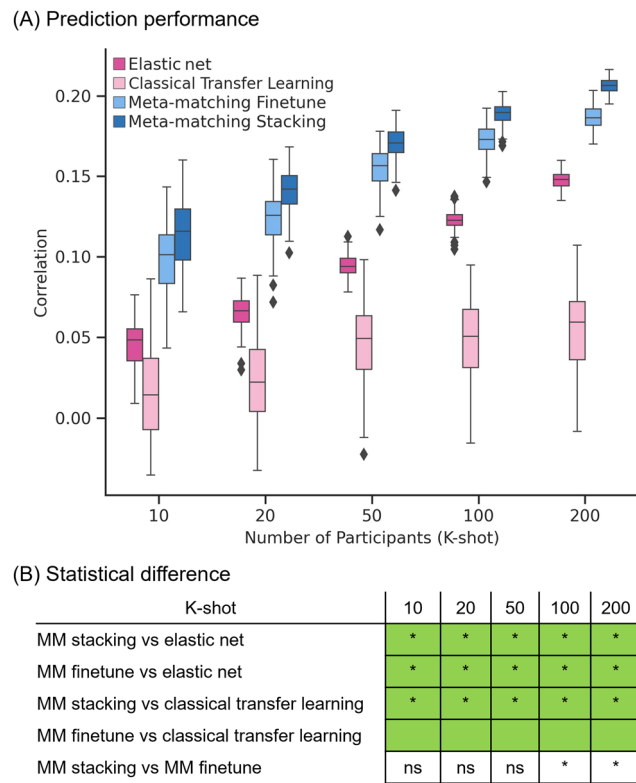


**Fig. 5.** Meta-matching compared favorably with elastic net and direct transfer learning in terms of Pearson's correlation within the UK Biobank. (A) Phenotypic prediction performance (Pearson's correlation) averaged across 34 meta-test phenotypes in the UK Biobank. X-axis represents the number of participants in the meta-test set of the UK Biobank used to train an elastic net or adapt the pretrained model from the meta-training set of the UK Biobank. Each boxplot shows the distribution of performance over 100 repetitions of sampling K participants. (B) Statistical difference between the prediction performance (Pearson's correlation) of baseline methods and meta-matching algorithms. p Values were calculated based on a two-sided bootstrapping test. "\*" indicates statistical significance after multiple comparisons correction (FDR  $q < 0.05$ ). "ns" indicates that statistical test did not survive FDR correction. We note that there was no statistical test between meta-matching finetune and classical transfer learning because the bootstrapping procedure was too expensive for the two methods. Colors indicate effect sizes of differences (Cohen's D) between approaches. Light green indicates effect size  $\geq 0.8$ . Dark green indicates  $0 \leq \text{effect size} < 0.8$ . Dark pink indicates  $-0.8 < \text{effect size} < 0$ . Light pink indicates effect size  $\leq -0.8$ . There is no color for the comparison between meta-matching finetune and stacking since they are both our proposed methods.

### 3.2. Meta-matching outperforms baselines in the HCP-YA dataset

The previous experiment results (Figs. 5 and 6) suggest that meta-matching can perform well when transferring within the same dataset (UK Biobank). We now evaluate the generalizability of meta-matching across datasets,

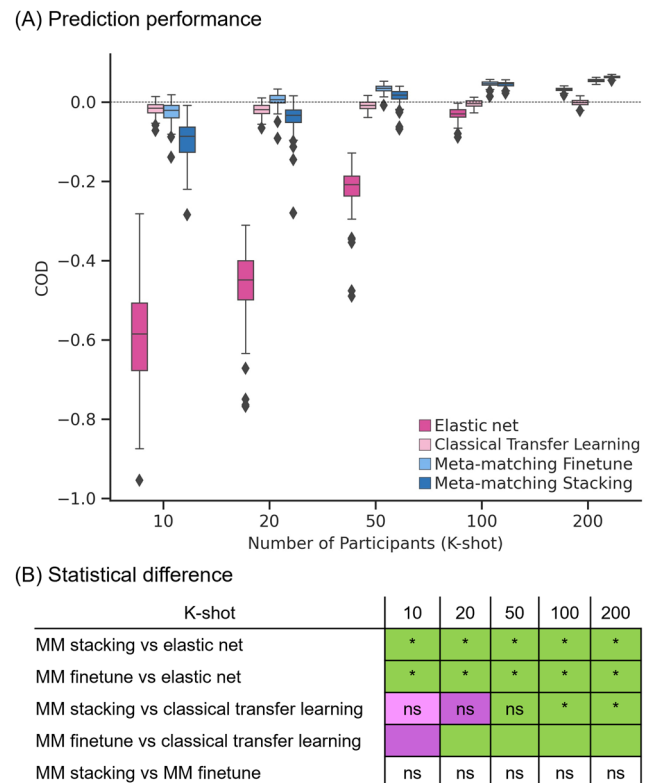


**Fig. 6.** Meta-matching compared favorably with elastic net and direct transfer learning in terms of coefficient of determination (COD) within the UK Biobank. (A) Phenotypic prediction performance (COD) averaged across 34 meta-test phenotypes in the UK Biobank. X-axis represents the number of participants in the meta-test set of the UK Biobank used to train an elastic net or adapt the pretrained model from the meta-training set of the UK Biobank. Each boxplot shows the distribution of performance over 100 repetitions of sampling K participants. (B) Statistical difference between the prediction performance (COD) of baseline methods and meta-matching algorithms. p Values were calculated based on a two-sided bootstrapping test. "\*" indicates statistical significance after multiple comparisons correction (FDR  $q < 0.05$ ). "ns" indicates statistical test did not survive FDR correction. We note that there was no statistical test between meta-matching finetune and classical transfer learning because the bootstrapping procedure was too expensive for the two methods. Colors indicate effect sizes of differences (Cohen's D) between approaches. Light green indicates effect size  $\geq 0.8$ . Dark green indicates  $0 \leq \text{effect size} < 0.8$ . Dark pink indicates  $-0.8 < \text{effect size} < 0$ . Light pink indicates effect size  $\leq -0.8$ . There is no color for the comparison between meta-matching finetune and stacking since they are both our proposed methods.

using the HCP-YA and HCP-Aging datasets (Fig. 2) in the following section and next section, respectively.

Figures 7A and 8A show the Pearson's correlation and COD, respectively, averaged across all 35 meta-test phenotypes in the HCP-YA dataset. Each boxplot represents 100 random samplings of K participants. Figure 9A shows

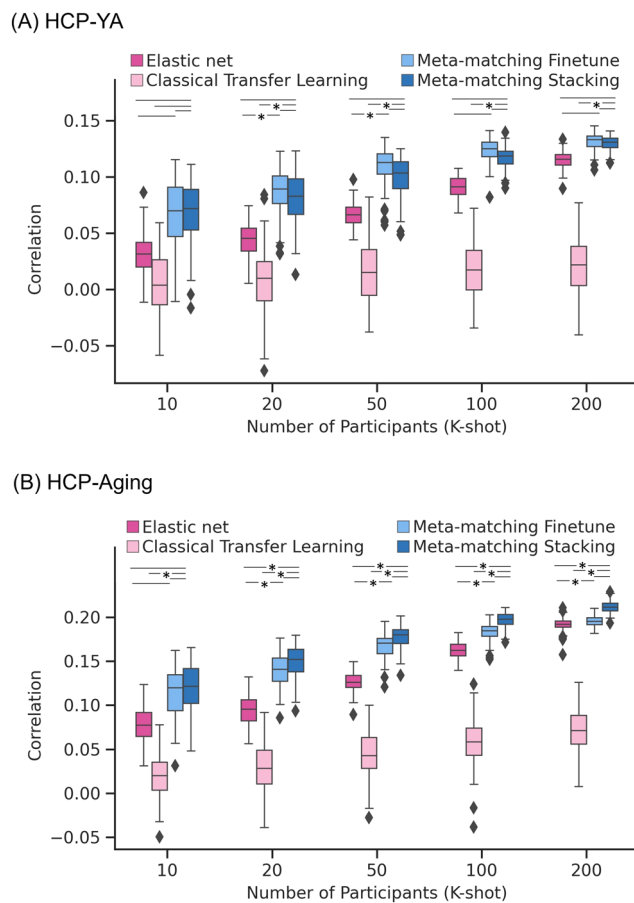


**Fig. 7.** Meta-matching compared favorably with elastic net and classical transfer learning in terms of Pearson's correlation when translating models from the UK Biobank to new target datasets. (A) Phenotypic prediction performance (Pearson's correlation) averaged across 35 meta-test phenotypes in the HCP-YA dataset. X-axis represents the number of participants from the HCP-YA dataset used to train an elastic net or adapt the pretrained model from the meta-training set. Each boxplot shows the distribution of performance over 100 repetitions of sampling K participants. (B) Same plot as panel (A) except that the analyses were performed in the HCP-Aging dataset and averaged across the 45 meta-test HCP-Aging phenotypes. "\*\*\*" and dash line indicate the results of a two-sided bootstrapping statistical test between meta-matching variants and other approaches. "\*\*\*" indicates statistical significance after multiple comparisons correction (FDR  $q < 0.05$ ). The dash line (without the "\*\*\*") indicates that the comparison was not significant. We note that there was no statistical test between meta-matching finetune and classical transfer learning because the bootstrapping procedure was too expensive for the two methods.

the outcomes of the statistical tests obtained by a bootstrapping procedure (Supplementary Methods S2 and Figure S2). The actual p values are reported in Table S7. Colors indicate effect sizes of differences (Cohen's D) between approaches.

In the case of Pearson's correlation (Fig. 7A), both meta-matching finetune and meta-matching stacking

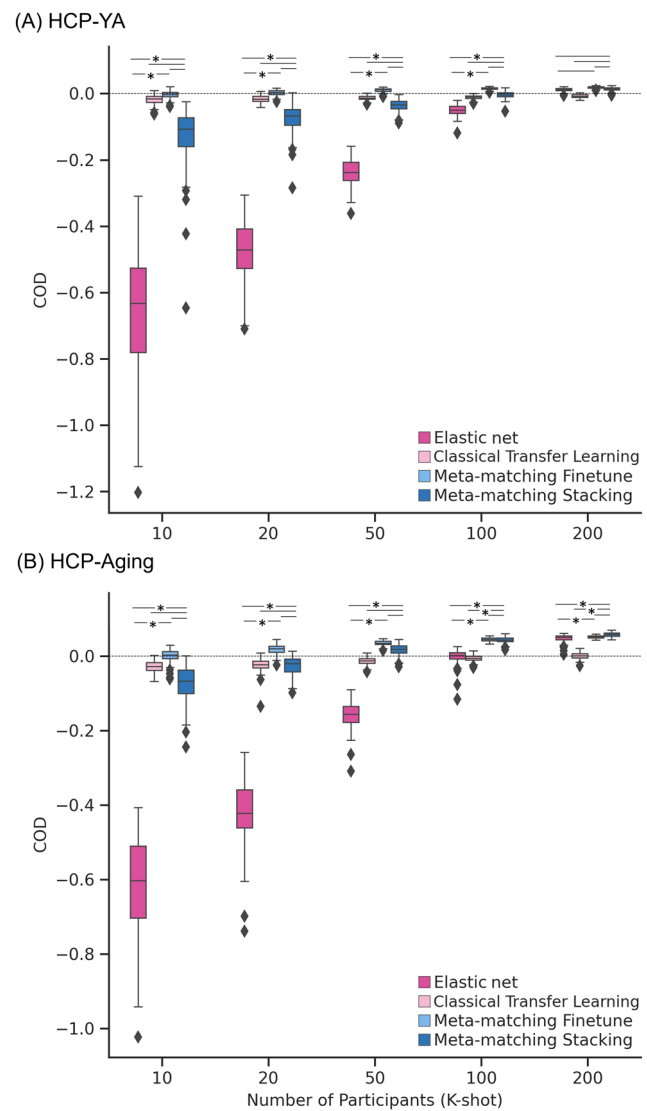


**Fig. 8.** Meta-matching compared favorably with elastic net and classical transfer learning in terms of coefficient of determination (COD) when translating models from the UK Biobank to new target datasets. (A) Phenotypic prediction performance (COD) averaged across 35 meta-test phenotypes in the HCP-YA dataset. X-axis represents the number of participants from the HCP-YA dataset used to train an elastic net or adapt the pretrained model from the meta-training set. Each boxplot shows the distribution of performance over 100 repetitions of sampling K participants. (B) Same plot as panel (A) except that the analyses were performed in the HCP-Aging dataset and averaged across the 45 meta-test HCP-Aging phenotypes. "\*\*\*" and dash line indicate the results of a two-sided bootstrapping statistical test between meta-matching variants and other approaches. "\*\*\*" indicates statistical significance after multiple comparisons correction (FDR  $q < 0.05$ ). The dash line (without the "\*\*\*") indicates that the comparison was not significant. We note that there was no statistical test between meta-matching finetune and classical transfer learning because the bootstrapping procedure was too expensive for the two methods.

(A) HCP-YA

K-shot	Correlation					COD				
	10	20	50	100	200	10	20	50	100	200
MM stacking vs elastic net	ns	ns	ns	ns	ns	*	*	*	*	ns
MM finetune vs elastic net	ns	*	*	ns	ns	*	*	*	*	ns
MM stacking vs transfer learning	ns	*	*	*	*	ns	ns	ns	ns	ns
MM finetune vs transfer learning										
MM stacking vs MM finetune	ns	ns	ns	ns	ns	ns	ns	ns	ns	ns

(B) HCP-Aging

K-shot	Correlation					COD				
	10	20	50	100	200	10	20	50	100	200
MM stacking vs elastic net	ns	*	*	*	*	*	*	*	*	*
MM finetune vs elastic net	ns	*	*	*	*	*	*	*	*	*
MM stacking vs transfer learning	*	*	*	*	*	ns	ns	ns	*	*
MM finetune vs transfer learning										
MM stacking vs MM finetune	ns	ns	ns	ns	ns	ns	ns	ns	ns	ns

**Fig. 9.** Statistical difference and effect size between the prediction performance of baseline methods and meta-matching algorithms for the (A) HCP-YA and (B) HCP-Aging datasets. p Values were calculated based on a two-sided bootstrapping test. “\*” indicates statistical significance after multiple comparisons correction (FDR  $q < 0.05$ ). “ns” indicates that statistical test did not survive FDR correction. We note that there was no statistical test between meta-matching finetune and classical transfer learning because the bootstrapping procedure was too expensive for the two methods. Colors indicate effect sizes of differences (Cohen’s D) between approaches. Light green indicates effect size  $\geq 0.8$ . Dark green indicates  $0 \leq \text{effect size} < 0.8$ . Dark pink indicates  $-0.8 < \text{effect size} < 0$ . Light pink indicates effect size  $\leq -0.8$ . There is no color for the comparison between meta-matching finetune and stacking since they are both our proposed methods.

were better than elastic net and classical transfer learning for all values of K with large effect sizes (light green in Fig. 9A). Meta-matching finetune was statistically better than elastic net for  $K = 20$  and  $50$ . Meta-matching stacking was statistically better than classical transfer learning for  $K \geq 20$ . For this cross-dataset analysis, meta-matching finetune was generally numerically better, but not statistically better than meta-matching stacking.

In the case of COD (Fig. 8A), both meta-matching finetune and meta-matching stacking greatly outperformed elastic net for  $K \leq 100$ . For  $K \leq 50$ , classical transfer learning was numerically better than meta-matching stacking with large effect sizes (light pink in Fig. 9A), but the differences were not significant. From  $K \geq 100$ , meta-matching stacking was numerically better, but not statistically better than transfer learning.

On the other hand, for all values of K, meta-matching finetune was numerically better than classical transfer learning with large effect sizes (light green in Fig. 9A). We note that there was no statistical test between meta-matching finetune and classical transfer learning

because of the huge computational cost of the two approaches, so no bootstrapping was performed for either approach.

Another relevant point is that COD for all approaches was negative (or almost zero) for  $K = 10$ , and only positive for meta-matching finetune for  $K \geq 20$ , suggesting that absolute prediction accuracy (i.e., COD) is difficult even with meta-learning or transfer learning when the sample size is very small.

Overall, meta-matching compared favorably with respect to elastic net for all values of K for both evaluation metrics (Pearson’s correlation and COD). On the other hand, meta-matching compared favorably with respect to transfer learning for all values of K for Pearson’s correlation and for  $K \geq 100$  for COD.

### 3.3. Meta-matching outperforms baselines in the HCP-Aging dataset

Figures 7B and 8B show the Pearson’s correlation and COD, respectively, averaged across all 45 meta-test



phenotypes in the HCP-Aging dataset. Each boxplot represents 100 random samplings of  $K$  participants. Figure 9B shows the outcomes of the statistical tests obtained by a bootstrapping procedure (Supplementary Methods S2 and Figure S3). The actual  $p$  values are reported in Table S8. Colors indicate effect sizes of differences (Cohen's  $D$ ) between approaches.

In the case of Pearson's correlation (Fig. 7B), both meta-matching finetune and meta-matching stacking greatly outperformed elastic net and classical transfer learning for most values of  $K$ . Meta-matching stacking was statistically better than elastic net for  $K \geq 20$ . Meta-matching stacking was statistically better than classical transfer learning for all values of  $K$ . For this cross-dataset analysis, meta-matching stacking was numerically better, but not statistically better than meta-matching finetune.

In the case of COD (Fig. 8B), both meta-matching finetune and meta-matching stacking greatly outperformed elastic net for all values of  $K$ . For  $K \leq 20$ , classical transfer learning was numerically better, but not statistically better than meta-matching stacking. From  $K \geq 50$ , meta-matching stacking was numerically better than transfer learning with statistical significance achieved for  $K \geq 100$ .

On the other hand, for all values of  $K$ , meta-matching finetune was numerically better than classical transfer learning with large effect sizes (light green in Fig. 9B). We note that there was no statistical test between meta-matching finetune and classical transfer learning because of the huge computational cost of the two approaches, so no bootstrapping was performed for either approach.

Another relevant point is that COD for all approaches was negative (or almost zero) for  $K = 10$ , and only positive for meta-matching finetune for  $K \geq 20$ , suggesting that absolute prediction accuracy (i.e., COD) is difficult even with meta-learning or transfer learning when the sample size is very small.

Overall, meta-matching was better than elastic net for all values of  $K$  for both evaluation metrics (Pearson's correlation and COD). On the other hand, meta-matching compared favorably with respect to transfer learning for all values of  $K$  for Pearson's correlation and for  $K \geq 50$  for COD.

### 3.4. Different improvements on different phenotypes

Overall, meta-matching improved prediction on average across multiple phenotypes. However, we note that the improvement was not uniform across phenotypes. Figure 10 illustrates the prediction performance (Pearson's correlation) of three nonbrain-imaging phenotypes for  $K = 100$  participants. In the case of the HCP-YA dataset (Fig. 10A), meta-matching finetune compared favorably

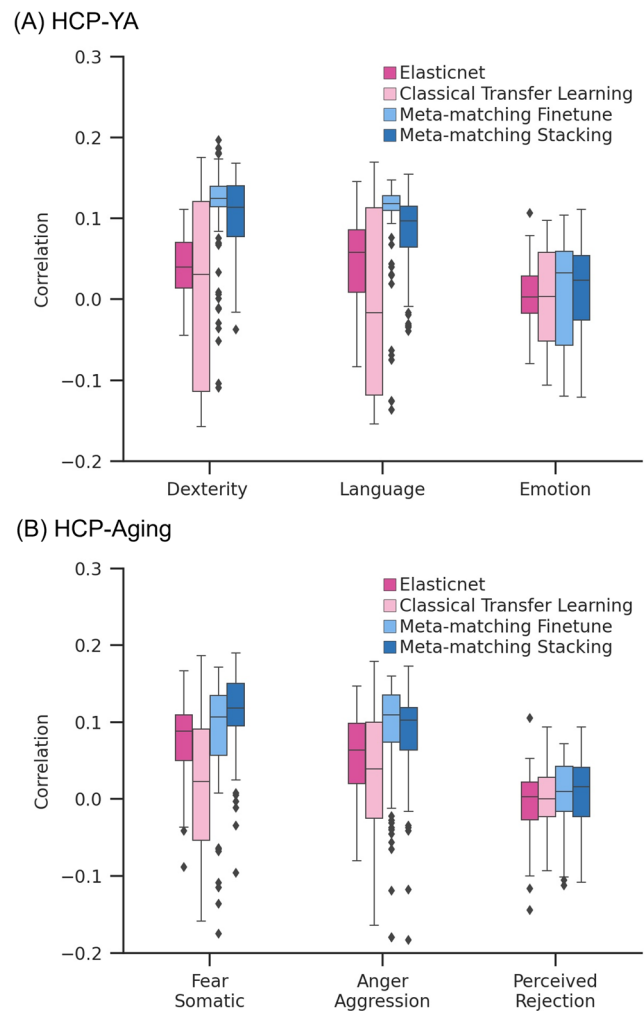


**Fig. 10.** Examples of prediction performance (Pearson's correlation) for different nonbrain-imaging phenotypes in the (A) HCP-YA and (B) HCP-Aging datasets in the case of  $K = 100$  participants.

with other approaches for predicting dexterity and language, but only achieved similar prediction accuracy on emotion. In the case of the HCP-Aging dataset (Fig. 10B), meta-matching stacking compared favorably with other approaches for predicting fear somatic and anger aggression, but only achieved similar prediction accuracy on perceived rejection. Tables S9 and S10 report the prediction accuracy (Pearson's correlation and COD) of all phenotypes in the HCP-YA and HCP-Aging datasets for all approaches. Tables S11 and S12 report the prediction errors (mean absolute error) for all phenotypes.

Given that meta-matching exploits correlations among phenotypes, we hypothesized that variability in prediction improvements was driven by interphenotype correlations between the meta-training and meta-test sets. Figure 11 shows the performance improvement (Pearson's correlation) of meta-matching stacking as a function of the maximum correlation between each meta-test

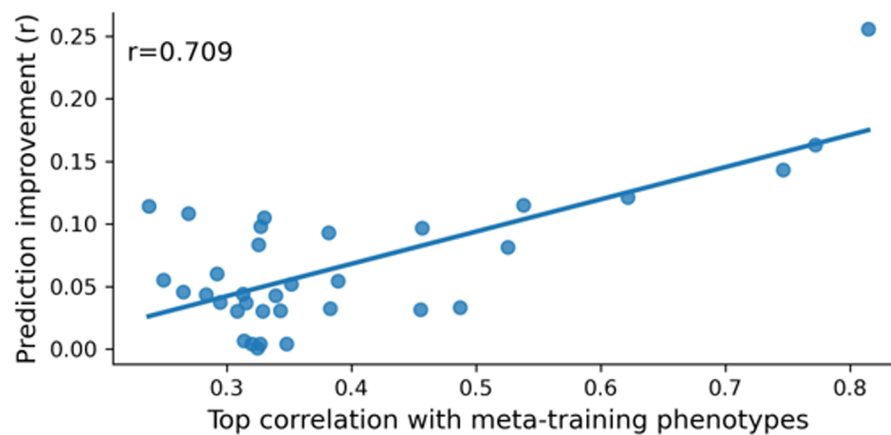


**Fig. 11.** Prediction improvements were driven by correlations between meta-training and meta-test phenotypes. Vertical axis shows the prediction improvement of meta-matching stacking with respect to elastic net baseline under the 100-shot scenario. Prediction performance was measured using Pearson's correlation. Each dot represents a meta-test phenotype. Horizontal axis shows each test phenotype's top absolute Pearson's correlation with phenotypes in the meta-training set. Test phenotypes with stronger correlations with at least one training phenotype led to greater prediction improvement with meta-matching.

phenotype and meta-training phenotype in the within-UK Biobank analysis. As expected, meta-test phenotypes with stronger correlations with at least one meta-training phenotype led to greater prediction improvement with meta-matching. We note that this analysis required meta-training and meta-test phenotypes to be present in the same participants, so could only be performed for the within-UK Biobank analysis.

### 3.5. Interpreting meta-matching stacking with Haufe transform

Figure 12 illustrates the feature importance maps obtained from the Haufe transform for predicting the Rey Auditory Verbal Learning Test (RAVLT) score and Montreal Cognitive Assessment (MOCA) in the HCP-Aging dataset for  $K = 100$ . We note that a higher RAVLT or MOCA scores indicated better cognition.

Since we are using T1 intensity for prediction, linking the feature importance values of T1 intensities to more neuroanatomically grounded interpretations has to be done with care. For both RAVLT and MOCA, positive feature importance values were observed in the ventral diencephalon and the third ventricle (left panels of Figure 12A and 12B), which suggested that higher T1 value led to prediction of better cognition (higher RAVLT and MOCA scores). By observing participants who performed poorly (right panels of Figure 12A and 12B) and participants who performed well (middle panels of Figure 12A and 12B), we inferred that the prediction might be partially driven by enlarged ventricles in participants with worse cognition (arrows in Fig. 12), yielding a lower T1 value in the region.

Similarly, we observed negative feature importance values on the edges of the left and right hippocampi (rather than directly on top of the hippocampi), which suggested that higher T1 value led to prediction of worse cognition (lower RAVLT and MOCA scores). By observing participants who performed poorly (right panels of Figure 12A and 12B) and participants who performed well (middle panels of Figure 12A and 12B), we inferred that the prediction might be partially driven by gray-matter loss at or near the hippocampi, yielding a higher T1 value in the region, consistent with the aging literature (Apostolova et al., 2012; Ritter et al., 2017).

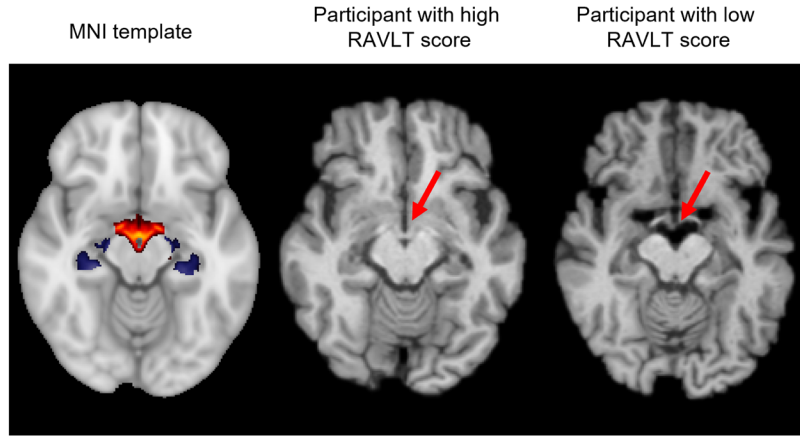
## 4. DISCUSSION

In this study, we adapted two meta-matching variants from our previous study (He et al., 2022) to translate prediction models trained from large-scale T1-weighted anatomical MRI datasets to predict new nonbrain-imaging phenotypes in small-scale T1-weighted anatomical MRI datasets. We demonstrated that meta-matching finetune and meta-matching stacking greatly outperformed classical elastic net and classical transfer learning when the number of participants  $\leq 200$ . Meta-matching performed well even when translating from a large-scale dataset (UK Biobank) to a small dataset (HCP-YA or HCP-Aging) with different scanners, acquisition, demographics, and preprocessing.

### 4.1. Benchmarking

Across all analyses in the UK Biobank, HCP-YA, and HCP-Aging datasets (Figs. 5 to 9), meta-matching

## (A) Predictive features of RAVLT



## (B) Predictive features of MOCA

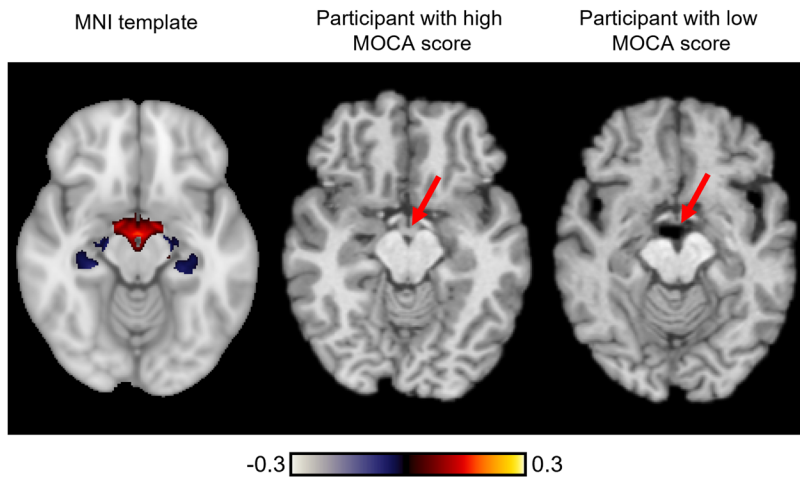


**Fig. 12.** Feature importance of meta-matching stacking in the HCP-Aging dataset for  $K = 100$  participants. (A) Feature importance map of meta-matching stacking from predicting Rey Auditory Verbal Learning Test (RAVLT) score. Left panel shows the feature importance map on the MNI152 template. A positive (or negative) feature importance value indicates that higher intensity was associated with predicting greater (or lower) phenotypic values. Middle panel shows an example participant with high RAVLT score. Right panel shows an example participant with low RAVLT score. (B) Feature importance map of meta-matching stacking from predicting the Montreal Cognitive Assessment (MOCA) score. Left panel shows the feature importance map on the MNI152 template. Middle panel shows an example participant with high MOCA score. Right panel shows an example participant with low MOCA score.

consistently outperformed elastic net across both evaluation metrics (correlation and COD). It is worth noting that the elastic net utilized thickness and volumetric measures generated by FreeSurfer, instead of the intensity values of T1 images (like meta-matching and transfer learning). One reason is that it is too computationally expensive to include a baseline elastic net with T1 image as input. Based on our back of the envelope calculations, just running such a baseline on HCP-Aging alone would require around 50 days of computation time on our computing facility. Furthermore, given that we are working in the small sample regime with  $K \leq 200$  training participants, we believe that the small number

of less than 200 predefined morphometric features together with elastic net provides a stronger baseline than an elastic net with T1 image as the input.

When using Pearson's correlation as an evaluation metric, transfer learning performed poorly with substantially worse performance than both meta-matching variants and even elastic net (Figs. 5, 7 and 9). On the other hand, when using COD as an evaluation metric, transfer learning was more competitive with respect to the other approaches (Figs. 6, 8, and 9). More specifically, transfer learning was numerically better (but not statistically better) than meta-matching stacking for small values of  $K$ , while meta-matching stacking was numerically better

(and sometimes statistically better) than transfer learning for larger values of  $K$ .

On the other hand, meta-matching finetune outperformed transfer learning for most values of  $K$  even in the case of COD. We note that meta-matching finetune is similar to classical transfer learning in the sense that the last two layers of the CNN were finetuned. However, while transfer learning initialized the last layer of the CNN from scratch (Section 2.3.2), meta-matching finetune retained the weights leading to the output node that predicted the  $K$  meta-test participants the best (for each meta-test phenotype). This further supported the importance of the meta-matching approach.

Overall, meta-matching stacking was the best for the Pearson's correlation metric, while meta-matching finetune was the best for COD. Pearson's correlation is a measure of relative prediction performance, while COD is a measure of absolute prediction performance (E. S. Finn et al., 2015; Poldrack et al., 2020; Scheinost et al., 2019). Therefore, researchers more focused on relative prediction performance might consider using meta-matching stacking, while researchers more focused on absolute prediction performance might consider using meta-matching finetune. Furthermore, all approaches achieved negative or close to zero COD when  $K \leq 20$ , suggesting that absolute prediction remains out of reach in the very small sample regime. COD was above zero for meta-matching finetune when  $K \geq 50$ . However, COD values were still less than 0.1 (i.e., 10% of explained variance) even when  $K = 200$ , suggesting potential room for improvement.

However, we note that the reported averaged COD values obscured large variation in prediction accuracies across phenotypes. In the case of HCP-Aging, when  $K = 100$  (Table S10), meta-matching finetune was able to achieve COD of more than 0.2 (i.e., more than 20% explained variance) for certain cognitive (e.g., processing speed) and physical (e.g., endurance) measures, while other phenotypes (e.g., positive affect) still could not achieve better than chance prediction ( $\text{COD} < 0$ ).

We also observe that prediction accuracy was generally higher in the HCP-Aging dataset than in the HCP-YA dataset. One reason might be because the UK Biobank comprised middle-aged and elderly participants, so might generalize better to elderly participants in the HCP-Aging dataset than young adults in the HCP-YA dataset. A second reason might be that the relationship between interindividual variability in brain structure and phenotypic measures is stronger in elderly participants than in younger adults because of the well-known effects of aging on brain structure (Jockwitz et al., 2019; Kuznetsova et al., 2016). Clear evidence for the second reason comes from the fact that the elastic net baseline

also performed better in the HCP-Aging dataset than in the HCP-YA dataset.

## 4.2. Interpreting meta-matching models

Meta-matching models can be interpreted at the level of imaging features by using the Haufe transform (Haufe et al., 2014). To illustrate this procedure, we applied the Haufe transform (Haufe et al., 2014) to the translated meta-matching stacking models in the HCP-Aging dataset (Fig. 12). For a given meta-test phenotype, Haufe transform was calculated as the covariance between the phenotype's prediction based on the meta-matching stacking model and the intensity value of each T1 voxel (across  $K$  participants), yielding a 3D volume. We found that poorer cognitive performance in terms of worse RAVLT and MOCA scores was related to greater gray-matter atrophy and larger ventricular size, which is consistent with the aging literature (Apostolova et al., 2012; Ritter et al., 2017). Meta-matching finetune can be interpreted in a similar fashion.

In addition to interpreting meta-matching models at the level of brain-imaging features, the meta-matching models can also be interpreted at the level of phenotypic traits. In the case of meta-matching stacking, this can again be achieved using the Haufe transform. To illustrate this, let us consider the pretrained 3D CNN model from the UK Biobank with 67 prediction outputs. This 3D CNN model can be translated to predict a new meta-test phenotype using  $K$  participants from the meta-test set using the stacking procedure. The Haufe transform can then be calculated as the covariance (across the  $K$  participants) between the phenotype's prediction from the final stacking model and the 67 inputs to the stacking model, yielding a vector of length 67, which indicates the relative importance of the original 67 meta-training phenotypes for predicting the meta-test phenotype.

## 4.3. Limitations and future work

Because meta-matching exploits correlations between the phenotypes of meta-training and meta-test sets, the amount of prediction improvement strongly relied on the strongest correlations between the meta-test phenotype and meta-training phenotypes (Fig. 11). Consequently, not all phenotypes might benefit from meta-matching. However, we note that this limitation exists for all meta-learning and transfer learning algorithms—model transfer is easier if the source and target domains are more similar; performance will degrade if source and target domains are very different.



The mismatch between meta-test and meta-training phenotypes can be accentuated by population differences or lack of diversity in the meta-training set (Greene et al., 2022; Li et al., 2022). Since our current study utilized a single source dataset (UK Biobank), the meta-matching models might not generalize as well to new populations, e.g., of different ethnicity or age. In our study, meta-matching still outperformed classical elastic net in young adults from North America (HCP-YA datasets), but we could potentially achieve even better results if meta-matching models were trained on a wider range of source datasets that included young adults from North America. An important future direction is to develop meta-matching models based on multiple diverse T1 datasets. We have recently developed meta-matching variants (dataset stacking and multilayer meta-matching) for resting-state functional connectivity (Chen et al., 2023), which could be adapted to T1 data.

Beyond RSFC from our previous studies (Chen et al., 2023; He et al., 2020) and T1 measures considered in this study, we can in principle extend meta-matching to other MRI modalities (e.g., diffusion MRI) and non-MRI data (e.g., electroencephalogram). Other T1 measures, such as surface area, sulcal depth, and curvature, could also be considered. Fusion of meta-matching models across modalities might potentially improve prediction performance, although we note that such an improvement is not a guaranteed outcome. For example, our previous study (Ooi et al., 2022) found that integrating T1, diffusion, and functional connectivity measures within a multikernel regression framework did not improve prediction accuracy in young healthy participants over just functional connectivity alone. However, this negative finding (Ooi et al., 2022) might not generalize to meta-matching and other populations. One tricky issue arising from multiple modality fusion is dealing with inevitable missing modality in a new test participant, which is still an unsolved problem.

Finally, in the current study, we trained our meta-matching model based on the FSL MNI152 template space because it is the most popular standard space in the literature and also because the major datasets (in this case, UK Biobank, HCP-Aging, HCP-YA) provide T1 data in that space. Researchers using other volumetric coordinate systems, e.g., Colin27 (Holmes et al., 1998) and SPM MNI152 (Mazziotta et al., 2001), might not be able to benefit as much from our models. However, unlike different RSFC atlases (Craddock et al., 2012; Gordon et al., 2016; Schaefer et al., 2018; Shen et al., 2013; Yan et al., 2023; Yeo et al., 2011), the different volumetric spaces are probably not as different. As such, it is entirely possible that our meta-matching procedure on the K participants in other coordinate systems (e.g., Colin27 or SPM

MNI152) might overcome atlas space differences, yielding good performance. We leave this to future work.

#### 4.4. Related studies

There has been a large number of studies using T1 MRI to predict individual-level phenotypic traits, clinical symptoms, and diagnostic categories (Arbabshirani et al., 2017; Bhagwat et al., 2019; Cohen et al., 2021; Ooi et al., 2022; Sabuncu et al., 2015). However, most of these studies focused on within-dataset prediction, without considering the generalization of their predictive models to new datasets (Wu et al., 2023). In more recent years, there is a growing number of studies adapting models trained on large datasets to predict the same phenotype in new data (Holderrieth et al., 2022; Jónsson et al., 2019), and more rarely, to predict a new phenotype in a new dataset (Leonardsen et al., 2022; Lu et al., 2022). This type of transfer learning or meta-learning is typically achieved by some form of finetuning of the model trained on one or more large-scale source datasets (Bae et al., 2021; Dhinagar et al., 2023; Wood et al., 2024), similar to our transfer learning baseline. As shown in our study, both meta-matching variants appeared to outperform this type of transfer learning.

## 5. CONCLUSION

In this study, we showed that meta-matching can be used to translate T1-based phenotypic prediction models from large source datasets to predict new phenotypes in small target datasets. By exploiting correlations between phenotypes, meta-matching greatly outperformed elastic net and classical transfer learning, both when translating models within the same dataset and when translating models across datasets with different MRI scanners, acquisition protocols, and demographics. Overall, our results demonstrated the versatility of the meta-matching framework.

## DATA AND CODE AVAILABILITY

The code used in this study can be found here ([https://github.com/ThomasYeoLab/CBIG/tree/master/stable\\_projects/predict\\_phenotypes/Naren2024\\_MMT1](https://github.com/ThomasYeoLab/CBIG/tree/master/stable_projects/predict_phenotypes/Naren2024_MMT1)). Two co-authors (Lijun An and Chen Zhang) reviewed the code before merging it into the GitHub repository to reduce the chance of coding errors. The trained models for meta-matching are also publicly available ([https://github.com/ThomasYeoLab/Meta\\_matching\\_models/tree/main/T1/v1.0](https://github.com/ThomasYeoLab/Meta_matching_models/tree/main/T1/v1.0)). This study used publicly available data from the UK Biobank (<https://www.ukbiobank.ac.uk/>), as well as

the HCP-YA and HCP-Aging datasets (<https://www.humanconnectome.org/>). Data can be accessed via data use agreements.

## AUTHOR CONTRIBUTIONS

N.W., L.A., C.Z., R.K., P.C., D.B., S.B.E., A.J.H., and B.T.T.Y. designed the research. N.W. conducted the research. N.W., L.A., C.Z., R.K., P.C., D.B., S.B.E., A.J.H., and B.T.T.Y. interpreted the results. N.W. and B.T.T.Y. wrote the manuscript and made the figures. N.W., L.A., and C.Z. reviewed and published the code. All authors contributed to project direction via discussion. All authors edited the manuscript.

## DECLARATION OF COMPETING INTEREST

The authors declare no competing interests.

## ACKNOWLEDGEMENTS

Our research is supported by the NUS Yong Loo Lin School of Medicine (NUHSRO/2020/124/TMR/LOA), the Singapore National Medical Research Council (NMRC) LCG (OFLCG19May-0035), NMRC CTG-IIT (CTGIIT23jan-0001), NMRC STaR (STaR20nov-0003), Singapore Ministry of Health (MOH) Centre Grant (CG21APR1009), the Temasek Foundation (TF2223-IMH-01), and the United States National Institutes of Health (R01MH120080 & R01MH133334). Our computational work was partially performed on resources of the National Supercomputing Centre, Singapore (<https://www.nsc.sg>). Any opinions, findings, and conclusions or recommendations expressed in this material are those of the authors and do not reflect the views of the Singapore NRF, NMRC, or MOH. This research has been conducted using the UK Biobank Resource under application number 25163, and the Human Connectome Project, WU-Minn Consortium (Principal Investigators: David Van Essen and Kamil Ugurbil; 1U54MH091657) funded by the 16 NIH Institutes and Centers that support the NIH Blueprint for Neuroscience Research, and the National Institute On Aging of the National Institutes of Health under Award Number U01AG052564 and by funds provided by the McDonnell Center for Systems Neuroscience at Washington University in St. Louis. The HCP-Aging 2.0 Release data used in this report came from DOI: 10.15154/1520707 and by the McDonnell Center for Systems Neuroscience at Washington University.

## SUPPLEMENTARY MATERIALS

Supplementary material for this article is available with the online version here: [https://doi.org/10.1162/imag\\_a\\_00251](https://doi.org/10.1162/imag_a_00251).

## REFERENCES

- Aderghal, K., Khvostikov, A., Krylov, A., Benois-Pineau, J., Afdel, K., & Catheline, G. (2018). Classification of Alzheimer disease on imaging modalities with deep CNNs using cross-modal transfer learning. *2018 IEEE 31st International Symposium on Computer-Based Medical Systems (CBMS)*, 345–350. <https://doi.org/10.1109/cbms.2018.00067>
- Alfaro-Almagro, F., Jenkinson, M., Bangerter, N. K., Andersson, J. L., Griffanti, L., Douaud, G., Sotiropoulos, S. N., Jbabdi, S., Hernandez-Fernandez, M., & Vallee, E. (2018). Image processing and quality control for the first 10,000 brain imaging datasets from UK Biobank. *NeuroImage*, 166, 400–424. <https://doi.org/10.1016/j.neuroimage.2017.10.034>
- Andrychowicz, M., Denil, M., Gomez, S., Hoffman, M. W., Pfau, D., Schaul, T., Shillingford, B., & De Freitas, N. (2016). Learning to learn by gradient descent by gradient descent. *Advances in Neural Information Processing Systems*, 29. <https://doi.org/10.48550/arXiv.1606.04474>
- Apostolova, L. G., Green, A. E., Babakchian, S., Hwang, K. S., Chou, Y.-Y., Toga, A. W., & Thompson, P. M. (2012). Hippocampal atrophy and ventricular enlargement in normal aging, mild cognitive impairment and Alzheimer's disease. *Alzheimer Disease and Associated Disorders*, 26(1), 17–27. <https://doi.org/10.1097/wad.0b013e3182163b62>
- Arbabshirani, M. R., Plis, S., Sui, J., & Calhoun, V. D. (2017). Single subject prediction of brain disorders in neuroimaging: Promises and pitfalls. *NeuroImage*, 145, 137–165. <https://doi.org/10.1016/j.neuroimage.2016.02.079>
- Bae, J., Stocks, J., Heywood, A., Jung, Y., Jenkins, L., Hill, V., Katsaggelos, A., Popuri, K., Rosen, H., & Beg, M. F. (2021). Transfer learning for predicting conversion from mild cognitive impairment to dementia of Alzheimer's type based on a three-dimensional convolutional neural network. *Neurobiology of Aging*, 99, 53–64. <https://doi.org/10.1016/j.neurobiolaging.2020.12.005>
- Bhagwat, N., Pipitone, J., Voineskos, A. N., Chakravarty, M. M., & Alzheimer's Disease Neuroimaging Initiative. (2019). An artificial neural network model for clinical score prediction in Alzheimer disease using structural neuroimaging measures. *Journal of Psychiatry and Neuroscience*, 44(4), 246–260. <https://doi.org/10.1503/jpn.180016>
- Bookheimer, S. Y., Salat, D. H., Terpstra, M., Ances, B. M., Barch, D. M., Buckner, R. L., Burgess, G. C., Curtiss, S. W., Diaz-Santos, M., & Elam, J. S. (2019). The lifespan human connectome project in aging: An overview. *NeuroImage*, 185, 335–348. <https://doi.org/10.1016/j.neuroimage.2018.10.009>
- Breiman, L. (1996). Stacked regressions. *Machine Learning*, 24, 49–64. <https://doi.org/10.1007/bf00117832>
- Bzdok, D., & Meyer-Lindenberg, A. (2018). Machine learning for precision psychiatry: Opportunities and challenges. *Biological Psychiatry Cognitive Neuroscience Neuroimaging*, 3(3), 223–230. <https://doi.org/10.1016/j.bpsc.2017.11.007>
- Chen, P., An, L., Wulan, N., Zhang, C., Zhang, S., Ooi, L. Q. R., Kong, R., Chen, J., Wu, J., & Chopra, S. (2023). Multilayer meta-matching: Translating phenotypic prediction models from multiple datasets to small data. *bioRxiv*. <https://doi.org/10.1101/2023.12.05.569848>
- Chu, C., Hsu, A.-L., Chou, K.-H., Bandettini, P., Lin, C., & Alzheimer's Disease Neuroimaging Initiative. (2012). Does feature selection improve classification accuracy? Impact of sample size and feature selection

- on classification using anatomical magnetic resonance images. *Neuroimage*, 60(1), 59–70. <https://doi.org/10.1016/j.neuroimage.2011.11.066>
- Cohen, S. E., Zantvoord, J. B., Wezenberg, B. N., Bockting, C. L., & van Wingen, G. A. (2021). Magnetic resonance imaging for individual prediction of treatment response in major depressive disorder: A systematic review and meta-analysis. *Translational Psychiatry*, 11(1), 168. <https://doi.org/10.1038/s41398-021-01286-x>
- Craddock, R. C., James, G. A., Holtzheimer III, P. E., Hu, X. P., & Mayberg, H. S. (2012). A whole brain fMRI atlas generated via spatially constrained spectral clustering. *Human Brain Mapping*, 33(8), 1914–1928. <https://doi.org/10.1002/hbm.21333>
- Cui, Z., & Gong, G. (2018). The effect of machine learning regression algorithms and sample size on individualized behavioral prediction with functional connectivity features. *Neuroimage*, 178, 622–637. <https://doi.org/10.1016/j.neuroimage.2018.06.001>
- Dawud, A. M., Yurtkan, K., & Oztoprak, H. (2019). Application of deep learning in neuroradiology: Brain haemorrhage classification using transfer learning. *Computational Intelligence and Neuroscience*, 2019(1), 4629859. <https://doi.org/10.1155/2019/4629859>
- Dhinagar, N. J., Thomopoulos, S. I., Rajagopalan, P., Stripelis, D., Ambite, J. L., Ver Steeg, G., & Thompson, P. M. (2023). Evaluation of transfer learning methods for detecting Alzheimer's disease with brain MRI. *18th International Symposium on Medical Information Processing and Analysis*. <https://doi.org/10.1101/2022.08.23.505030>
- Fei-Fei, L., Fergus, R., & Perona, P. (2006). One-shot learning of object categories. *IEEE Transactions on Pattern Analysis and Machine Intelligence*, 28(4), 594–611. <https://doi.org/10.1109/tpami.2006.79>
- Feilong, M., Guntupalli, J. S., & Haxby, J. V. (2021). The neural basis of intelligence in fine-grained cortical topographies. *Elife*, 10, e64058. <https://doi.org/10.7554/elife.64058>
- Finn, C., Abbeel, P., & Levine, S. (2017). Model-agnostic meta-learning for fast adaptation of deep networks. *International Conference on Machine Learning*. <https://doi.org/10.48550/arXiv.1703.03400>
- Finn, E. S., Shen, X., Scheinost, D., Rosenberg, M. D., Huang, J., Chun, M. M., Papademetris, X., & Constable, R. T. (2015). Functional connectome fingerprinting: Identifying individuals using patterns of brain connectivity. *Nature Neuroscience*, 18(11), 1664–1671. <https://doi.org/10.1038/nn.4135>
- Fischl, B., Salat, D. H., Busa, E., Albert, M., Dieterich, M., Haselgrove, C., Van Der Kouwe, A., Killiany, R., Kennedy, D., & Klaveness, S. (2002). Whole brain segmentation: Automated labeling of neuroanatomical structures in the human brain. *Neuron*, 33(3), 341–355. [https://doi.org/10.1016/s0896-6273\(02\)00569-x](https://doi.org/10.1016/s0896-6273(02)00569-x)
- Genon, S., Eickhoff, S. B., & Kharabian, S. (2022). Linking interindividual variability in brain structure to behaviour. *Nature Reviews Neuroscience*, 23(5), 307–318. <https://doi.org/10.1038/s41583-022-00584-7>
- Ghafoorian, M., Mehrtash, A., Kapur, T., Karssemeijer, N., Marchiori, E., Pesteie, M., Guttman, C. R., de Leeuw, F.-E., Tempny, C. M., & Van Ginneken, B. (2017). Transfer learning for domain adaptation in MRI: Application in brain lesion segmentation. *Medical Image Computing and Computer Assisted Intervention – MICCAI 2017: 20th International Conference*, Quebec City, QC, Canada, September 11–13, 2017, Proceedings, Part III 20, [https://doi.org/10.1007/978-3-319-66179-7\\_59](https://doi.org/10.1007/978-3-319-66179-7_59)
- Gifford, G., McCutcheon, R., & McGuire, P. (2020). Neuroimaging studies in people at clinical high risk for psychosis. In *Risk factors for psychosis* (pp. 167–182). Academic Press. <https://doi.org/10.1016/b978-0-12-813201-2.00009-0>
- Glasser, M. F., Sotiropoulos, S. N., Wilson, J. A., Coalson, T. S., Fischl, B., Andersson, J. L., Xu, J., Jbabdi, S., Webster, M., & Polimeni, J. R. (2013). The minimal preprocessing pipelines for the Human Connectome Project. *Neuroimage*, 80, 105–124. <https://doi.org/10.1016/j.neuroimage.2013.04.127>
- Gordon, E. M., Laumann, T. O., Adeyemo, B., Huckins, J. F., Kelley, W. M., & Petersen, S. E. (2016). Generation and evaluation of a cortical area parcellation from resting-state correlations. *Cerebral Cortex*, 26(1), 288–303. <https://doi.org/10.1093/cercor/bhu239>
- Greene, A. S., Shen, X., Noble, S., Horien, C., Hahn, C. A., Arora, J., Tokoglu, F., Spann, M. N., Carrión, C. I., & Barron, D. S. (2022). Brain-phenotype models fail for individuals who defy sample stereotypes. *Nature*, 609(7925), 109–118. <https://doi.org/10.1038/s41586-022-05118-w>
- Harms, M. P., Somerville, L. H., Ances, B. M., Andersson, J., Barch, D. M., Bastiani, M., Bookheimer, S. Y., Brown, T. B., Buckner, R. L., & Burgess, G. C. (2018). Extending the Human Connectome Project across ages: Imaging protocols for the Lifespan Development and Aging projects. *NeuroImage*, 183, 972–984. <https://doi.org/10.1016/j.neuroimage.2018.09.060>
- Haufe, S., Meinecke, F., Görgen, K., Dähne, S., Haynes, J.-D., Blankertz, B., & Bießmann, F. (2014). On the interpretation of weight vectors of linear models in multivariate neuroimaging. *NeuroImage*, 87, 96–110. <https://doi.org/10.1016/j.neuroimage.2013.10.067>
- He, T., An, L., Chen, P., Chen, J., Feng, J., Bzdok, D., Holmes, A. J., Eickhoff, S. B., & Yeo, B. T. (2022). Meta-matching as a simple framework to translate phenotypic predictive models from big to small data. *Nature Neuroscience*, 25(6), 795–804. <https://doi.org/10.1038/s41593-022-01059-9>
- He, T., Kong, R., Holmes, A. J., Nguyen, M., Sabuncu, M. R., Eickhoff, S. B., Bzdok, D., Feng, J., & Yeo, B. T. (2020). Deep neural networks and kernel regression achieve comparable accuracies for functional connectivity prediction of behavior and demographics. *Neuroimage*, 206, 116276. <https://doi.org/10.1016/j.neuroimage.2019.116276>
- Holderrieth, P., Smith, S., & Peng, H. (2022). Transfer learning for neuroimaging via re-use of deep neural network features. *medRxiv*, 2022.2012.2011.22283324. <https://doi.org/10.1101/2022.12.11.22283324>
- Holmes, C. J., Hoge, R., Collins, L., Woods, R., Toga, A. W., & Evans, A. C. (1998). Enhancement of MR images using registration for signal averaging. *Journal of Computer Assisted Tomography*, 22(2), 324–333. <https://doi.org/10.1097/00004728-199803000-00032>
- Hospedales, T., Antoniou, A., Micaelli, P., & Storkey, A. (2021). Meta-learning in neural networks: A survey. *IEEE Transactions on Pattern Analysis and Machine Intelligence*, 44(9), 5149–5169. <https://doi.org/10.1109/tpami.2021.3079209>
- Jenkinson, M., Bannister, P., Brady, M., & Smith, S. (2002). Improved optimization for the robust and accurate linear registration and motion correction of brain images. *NeuroImage*, 17(2), 825–841. <https://doi.org/10.1006/nimg.2002.1132>
- Jenkinson, M., & Smith, S. (2001). A global optimisation method for robust affine registration of brain images.



- Medical Image Analysis*, 5(2), 143–156. [https://doi.org/10.1016/s1361-8415\(01\)00036-6](https://doi.org/10.1016/s1361-8415(01)00036-6)
- Jockwitz, C., Mérillat, S., Liem, F., Oschwald, J., Amunts, K., Caspers, S., & Jäncke, L. (2019). Generalizing age effects on brain structure and cognition: A two-study comparison approach. *Human Brain Mapping*, 40(8), 2305–2319. <https://doi.org/10.1002/hbm.24524>
- Jónsson, B. A., Bjornsdottir, G., Thorgeirsson, T., Ellingsen, L. M., Walters, G. B., Gudbjartsson, D., Stefansson, H., Stefansson, K., & Ulfarsson, M. (2019). Brain age prediction using deep learning uncovers associated sequence variants. *Nature Communications*, 10(1), 5409. <https://doi.org/10.1038/s41467-019-13163-9>
- Kebets, V., Holmes, A. J., Orban, C., Tang, S., Li, J., Sun, N., Kong, R., Poldrack, R. A., & Yeo, B. T. (2019). Somatosensory-motor dysconnectivity spans multiple transdiagnostic dimensions of psychopathology. *Biological Psychiatry*, 86(10), 779–791. <https://doi.org/10.1016/j.biopsych.2019.06.013>
- Klein, A., & Tourville, J. (2012). 101 labeled brain images and a consistent human cortical labeling protocol. *Frontiers in Neuroscience*, 6, 171. <https://doi.org/10.3389/fnins.2012.00171>
- Kuznetsova, K. A., Maniega, S. M., Ritchie, S. J., Cox, S. R., Storkey, A. J., Starr, J. M., Wardlaw, J. M., Deary, I. J., & Bastin, M. E. (2016). Brain white matter structure and information processing speed in healthy older age. *Brain Structure and Function*, 221, 3223–3235. <https://doi.org/10.1007/s00429-015-1097-5>
- Leonardsen, E., Peng, H., Kaufmann, T., Agartz, I., Andreassen, O., Celius, E., Espeseth, T., Harbo, H., Høgestøl, E., & de Lange, A. (2022). Deep neural networks learn general and clinically relevant representations of the ageing brain. *NeuroImage*, 256, Article 119210. <https://doi.org/10.1016/j.neuroimage.2022.119210>
- Li, J., Bzdok, D., Chen, J., Tam, A., Ooi, L. Q. R., Holmes, A. J., Ge, T., Patil, K. R., Jabbi, M., & Eickhoff, S. B. (2022). Cross-ethnicity/race generalization failure of behavioral prediction from resting-state functional connectivity. *Science Advances*, 8(11), eabj1812. <https://doi.org/10.1126/sciadv.abj1812>
- Long, J., Shelhamer, E., & Darrell, T. (2015). Fully convolutional networks for semantic segmentation. *Proceedings of the IEEE conference on computer vision and pattern recognition*, 3431–3440. <https://doi.org/10.1109/cvpr.2015.7298965>
- Lu, B., Li, H.-X., Chang, Z.-K., Li, L., Chen, N.-X., Zhu, Z.-C., Zhou, H.-X., Li, X.-Y., Wang, Y.-W., & Cui, S.-X. (2022). A practical Alzheimer's disease classifier via brain imaging-based deep learning on 85,721 samples. *Journal of Big Data*, 9(1), 101. <https://doi.org/10.1186/s40537-022-00650-y>
- Marek, S., Tervo-Clemmens, B., Calabro, F. J., Montez, D. F., Kay, B. P., Hatoum, A. S., Donohue, M. R., Foran, W., Miller, R. L., & Hendrickson, T. J. (2022). Reproducible brain-wide association studies require thousands of individuals. *Nature*, 603(7902), 654–660. <https://doi.org/10.1038/s41586-022-04492-9>
- Masouleh, S. K., Eickhoff, S. B., Hoffstaedter, F., Genon, S., & Alzheimer's Disease Neuroimaging Initiative. (2019). Empirical examination of the replicability of associations between brain structure and psychological variables. *elife*, 8, e43464. <https://doi.org/10.7554/elife.43464>
- Mazziotta, J., Toga, A., Evans, A., Fox, P., Lancaster, J., Zilles, K., Woods, R., Paus, T., Simpson, G., & Pike, B. (2001). A probabilistic atlas and reference system for the human brain: International Consortium for Brain Mapping (ICBM). *Philosophical Transactions of the Royal Society of London. Series B: Biological Sciences*, 356(1412), 1293–1322. <https://doi.org/10.1098/rstb.2001.0915>
- Mehmood, A., Yang, S., Feng, Z., Wang, M., Ahmad, A. S., Khan, R., Maqsood, M., & Yaqub, M. (2021). A transfer learning approach for early diagnosis of Alzheimer's disease on MRI images. *Neuroscience*, 460, 43–52. <https://doi.org/10.1016/j.neuroscience.2021.01.002>
- Miller, K. L., Alfaro-Almagro, F., Bangerter, N. K., Thomas, D. L., Yacoub, E., Xu, J., Bartsch, A. J., Jbabdi, S., Sotiropoulos, S. N., & Andersson, J. L. (2016). Multimodal population brain imaging in the UK Biobank prospective epidemiological study. *Nature Neuroscience*, 19(11), 1523–1536. <https://doi.org/10.1038/nn.4393>
- Ooi, L. Q. R., Chen, J., Zhang, S., Kong, R., Tam, A., Li, J., Dhamala, E., Zhou, J. H., Holmes, A. J., & Yeo, B. T. (2022). Comparison of individualized behavioral predictions across anatomical, diffusion and functional connectivity MRI. *NeuroImage*, 263, 119636. <https://doi.org/10.1016/j.neuroimage.2022.119636>
- Paszke, A., Gross, S., Chintala, S., Chanan, G., Yang, E., DeVito, Z., Lin, Z., Desmaison, A., Antiga, L., & Lerer, A. (2017). Automatic differentiation in pytorch. *31st Conference on Neural Information Processing Systems (NIPS 2017)*, Long Beach, CA, USA. <https://openreview.net/forum?id=BJJsrnfCZ>
- Peng, H., Gong, W., Beckmann, C. F., Vedaldi, A., & Smith, S. M. (2021). Accurate brain age prediction with lightweight deep neural networks. *Medical Image Analysis*, 68, 101871. <https://doi.org/10.1016/j.media.2020.101871>
- Pervaiz, U., Vidaurre, D., Woolrich, M. W., & Smith, S. M. (2020). Optimising network modelling methods for fMRI. *NeuroImage*, 211, 116604. <https://doi.org/10.1016/j.neuroimage.2020.116604>
- Poldrack, R. A., Huckins, G., & Varoquaux, G. (2020). Establishment of best practices for evidence for prediction: A review. *JAMA Psychiatry*, 77(5), 534–540. <https://doi.org/10.1001/jamapsychiatry.2019.3671>
- Ravi, S., & Larochelle, H. (2016). Optimization as a model for few-shot learning. *International Conference on Learning Representations*. <https://openreview.net/forum?id=rJY0-Kcll>
- Ritter, A., Hawley, N., Banks, S. J., & Miller, J. B. (2017). The association between Montreal Cognitive Assessment memory scores and hippocampal volume in a neurodegenerative disease sample. *Journal of Alzheimer's Disease*, 58(3), 695–699. <https://doi.org/10.3233/jad-161241>
- Sabuncu, M. R., Konukoglu, E., & Alzheimer's Disease Neuroimaging Initiative. (2015). Clinical prediction from structural brain MRI scans: A large-scale empirical study. *Neuroinformatics*, 13, 31–46. <https://doi.org/10.1007/s12021-014-9238-1>
- Schaefer, A., Kong, R., Gordon, E. M., Laumann, T. O., Zuo, X.-N., Holmes, A. J., Eickhoff, S. B., & Yeo, B. T. (2018). Local-global parcellation of the human cerebral cortex from intrinsic functional connectivity MRI. *Cerebral Cortex*, 28(9), 3095–3114. <https://doi.org/10.1093/cercor/bhx179>
- Scheinost, D., Noble, S., Horien, C., Greene, A. S., Lake, E. M., Salehi, M., Gao, S., Shen, X., O'Connor, D., & Barron, D. S. (2019). Ten simple rules for predictive modeling of individual differences in neuroimaging. *NeuroImage*, 193, 35–45. <https://doi.org/10.1016/j.neuroimage.2019.02.057>
- Schulz, M.-A., Yeo, B. T., Vogelstein, J. T., Mourao-Miranada, J., Kather, J. N., Kording, K., Richards, B.,



- & Bzdok, D. (2020). Different scaling of linear models and deep learning in UKBiobank brain images versus machine-learning datasets. *Nature Communications*, 11(1), 4238. <https://doi.org/10.1038/s41467-020-18037-z>
- Shen, X., Tokoglu, F., Papademetris, X., & Constable, R. T. (2013). Groupwise whole-brain parcellation from resting-state fMRI data for network node identification. *Neuroimage*, 82, 403–415. <https://doi.org/10.1016/j.neuroimage.2013.05.081>
- Simonyan, K., & Zisserman, A. (2014). Very deep convolutional networks for large-scale image recognition. *arXiv preprint arXiv:1409.1556*. <https://doi.org/10.1063/pt.5.028530>
- Smith, S. M., Nichols, T. E., Vidaurre, D., Winkler, A. M., Behrens, T. E., Glasser, M. F., Ugurbil, K., Barch, D. M., Van Essen, D. C., & Miller, K. L. (2015). A positive-negative mode of population covariation links brain connectivity, demographics and behavior. *Nature Neuroscience*, 18(11), 1565–1567. <https://doi.org/10.1038/nn.4125>
- Sudlow, C., Gallacher, J., Allen, N., Beral, V., Burton, P., Danesh, J., Downey, P., Elliott, P., Green, J., & Landray, M. (2015). UK biobank: An open access resource for identifying the causes of a wide range of complex diseases of middle and old age. *PLoS Medicine*, 12(3), e1001779. <https://doi.org/10.1371/journal.pmed.1001779>
- Talo, M., Baloglu, U. B., Yildirim, Ö., & Acharya, U. R. (2019). Application of deep transfer learning for automated brain abnormality classification using MR images. *Cognitive Systems Research*, 54, 176–188. <https://doi.org/10.1016/j.cogsys.2018.12.007>
- Van Essen, D. C., Smith, S. M., Barch, D. M., Behrens, T. E., Yacoub, E., Ugurbil, K., & Consortium, W.-M. H. (2013). The WU-Minn human connectome project: An overview. *NeuroImage*, 80, 62–79. <https://doi.org/10.1016/j.neuroimage.2013.05.041>
- Vanschoren, J. (2019). Meta-learning. In F. Hutter, L. Kotthoff, & J. Vanschoren (Eds.), *Automated machine learning: methods, systems, challenges* (pp. 35–61). Springer. [https://doi.org/10.1007/978-3-030-05318-5\\_2](https://doi.org/10.1007/978-3-030-05318-5_2)
- Wee, C.-Y., Liu, C., Lee, A., Poh, J. S., Ji, H., Qiu, A., & Alzheimers Disease Neuroimage Initiative. (2019). Cortical graph neural network for AD and MCI diagnosis and transfer learning across populations. *NeuroImage: Clinical*, 23, 101929. <https://doi.org/10.1016/j.nicl.2019.101929>
- Weiss, K., Khoshgoftaar, T. M., & Wang, D. (2016). A survey of transfer learning. *Journal of Big data*, 3(1), 1–40. <https://doi.org/10.1186/s40537-016-0043-6>
- Wolpert, D. H. (1992). Stacked generalization. *Neural Networks*, 5(2), 241–259. [https://doi.org/10.1016/s0893-6080\(05\)80023-1](https://doi.org/10.1016/s0893-6080(05)80023-1)
- Wood, D. A., Townend, M., Guilhem, E., Kafiabadi, S., Hammam, A., Wei, Y., Al Busaidi, A., Mazumder, A., Sasieni, P., & Barker, G. J. (2024). Optimising brain age estimation through transfer learning: A suite of pre-trained foundation models for improved performance and generalisability in a clinical setting. *Human Brain Mapping*, 45(4), e26625. <https://doi.org/10.1002/hbm.26625>
- Wu, J., Li, J., Eickhoff, S. B., Scheinost, D., & Genon, S. (2023). The challenges and prospects of brain-based prediction of behaviour. *Nature Human Behaviour*, 7(8), 1255–1264. <https://doi.org/10.1038/s41562-023-01670-1>
- Xia, C. H., Ma, Z., Ciric, R., Gu, S., Betzel, R. F., Kaczkurkin, A. N., Calkins, M. E., Cook, P. A., García de la Garza, A., & Vandekar, S. N. (2018). Linked dimensions of psychopathology and connectivity in functional brain networks. *Nature Communications*, 9(1), 3003. <https://doi.org/10.1038/s41467-018-05317-y>
- Yan, X., Kong, R., Xue, A., Yang, Q., Orban, C., An, L., Holmes, A. J., Qian, X., Chen, J., & Zuo, X.-N. (2023). Homotopic local-global parcellation of the human cerebral cortex from resting-state functional connectivity. *Neuroimage*, 273, 120010. <https://doi.org/10.1016/j.neuroimage.2023.120010>
- Yeo, B. T., Krienen, F. M., Sepulcre, J., Sabuncu, M. R., Lashkari, D., Hollinshead, M., Roffman, J. L., Smoller, J. W., Zöllei, L., & Polimeni, J. R. (2011). The organization of the human cerebral cortex estimated by intrinsic functional connectivity. *Journal of Neurophysiology*, 106(3), 1125–1165. <https://doi.org/10.1152/jn.00338.2011>
- Zou, H., & Hastie, T. (2005). Regularization and variable selection via the elastic net. *Journal of the Royal Statistical Society: Series B (Statistical Methodology)*, 67(2), 301–320. <https://doi.org/10.1111/j.1467-9868.2005.00503.x>